MODAL TESTING OF A RETROFITTED BUILDING

by

Ziya Dalkılıç

B.S, Civil Engineering, Boğaziçi University, 2010

Submitted to the Institute for Graduate Studies in
Science and Engineering in partial fulfillment of
the requirements for the degree of
Master of Science

Graduate Program in Civil Engineering

Boğaziçi University

2013

ACKNOWLEDGEMENTS

Firm and reassuring support of my loving parents needs to be distinctly addressed. For their unconditional affection, I've been and I'm under a non-repayable debt of gratitude.

I owe thanks to my thesis supervisor, Assist. Prof. Serdar Soyöz, for his tolerance and concern over the years.

GNU Octave software, freely available as part of the Free Software Foundation's GNU project, is extensively used as a scripting language in production of the computer algorithms of this study. A wide variety of extension packages for GNU Octave is made available through volunteering professionals from various disciplines. I feel obliged to thank these individuals for their compassion and valuable work.

I'd like to thank to Mr. Suat Başer from COMPUTERS & ENGINEERING for providing his help during the pre-purchase period of CSI Berkley's software licenses. On this issue, I owe thanks to Assist. Prof. Serdar Soyöz, also.

Lastly, B.Ü. Yapı İşleri ve Teknik Daire Başkanlığı shall be mentioned for going through the archives and lending me the original architectural drawings of ETA-B building.

ABSTRACT

MODAL TESTING OF A RETROFITTED BUILDING

ETA-B Building located in Boğaziçi University, North Campus is monitored before, during and after its retrofitting process by previous researchers. An Enhanced Frequency Domain Decomposition identification algorithm is developed in this study to be able to analyse the gathered data. The results of these analysis is then used along with the Finite Element Models generated in this study to perform model updating procedures. The updated and non-updated Finite Element Models are then subjected to linear time history analysis for a selection of earthquakes and the storey drift ratios are compared to evaluate the effect of Structural Health Monitoring on the obtained results. The results indicate that Structural Health Monitoring could have a distinct impact on the decision making process for safety approval, retrofitting or demolishing decisions for existing structures. The theory and background for Structural Health Monitoring is also made available in this thesis, along with discussions on what it could and could not currently enable in terms of its possible uses, advantages and shortcomings.

ÖZET

GÜÇLENDİRİLMİŞ BİR BİNANIN MODAL TESTİ

Boğaziçi Üniversitesi, Kuzey kampüsünde bulunan ETA-B binası geçirdiği güçlendirme projesi öncesinde, dahilinde ve sonrasında geçmiş araştırmacılar tarafından gözlemlenmiş ve ivme kayıtları elde edilmiştir. Bu kayıtların incelenebilmesi amacıyla bu çalışma dahilinde bir frekans uzayında tanımlama algoritması geliştirilmiş ve verilerin analizinde kullanılmıştır. Elde edilen analiz sonuçları bina için geliştirilen sonlu elemen modelleri ile birlikte bir model güncelleştirme çalışmasında kullanılmış ve analiz sonuçlarına göre güncellenmiştir. Güncelleştirilmiş ve güncelleştirilmemiş modeller daha sonra seçilen deprem ivme kayıtları için doğrusal zaman tanımlı deprem analizlerine tabi tutulmuş ve sonuçlar yapısal sağlık taramasının analiz sonuçlarına etkileri açısından kıyaslanmıştır. Sonuçlar yapısal sağlık taraması çalışmalarının binaların güvenilirlik onayının verilmesi, güçlendirilmesi veya yıkılması için verilecek olan kararlarda oldukça etkili olabileceğini göstermiştir. Bu çalışma dahilinde yapısal sağlık taraması ile ilgili gerekli teknik bilgi ve temele de yer verilmiş, bununla birlikte yapısal sağlık taramasının günümüzde sağlayabileceği ve sağlayamayacağı farklı kullanım alanları, faydalar ve eksiklikler tartışılmıştır.

TABLE OF CONTENTS

LIST OF FIGURES

LIST OF TABLES

LIST OF SYMBOLS

c	Viscous damping coefficient
dt	Time step
dw	Frequency step
D	Storey drift ratio
E	Young's modulus
$E[x]$	Expected value of x
$F\{\dots\}$	Fourier transform
$F^{-1}\{\dots\}$	Inverse Fourier transform
$F(t)$	Forcing function
i	Imaginary unit value, $\sqrt{-1}$
I	Area moment of inertia
$[I]$	Identity matrix
j	Discrete time index
k	Discrete frequency index or stiffness
m	Mass
N	Number of data points
N_{dof}	Number of degrees of freedom
$q(t)$	Modal motion displacement
$\dot{q}(t)$	Modal motion velocity
$\ddot{q}(t)$	Modal motion acceleration
R	Correlation function
S	Power spectral density function
SF	Sampling frequency
t	Continuous time
T	Period
t_j	Discrete time indexed with j
$u(t)$	Displacement
$\dot{u}(t)$	Velocity

$\ddot{u}(t)$	Acceleration
w	Continuous frequency
w_d	Damped natural frequency
w_k	Discrete frequency indexed with k
w_n	nth natural frequency
ξ	Damping ratio
ϕ_n	nth mode shape vector
$[\Phi]$	Modal matrix
ψ	Curvature

LIST OF ACRONYMS/ABBREVIATIONS

CAD	Computer Aided Design
DFT	Discrete Fourier Transform
EFDD	Enhanced Frequency Domain Decomposition
FDD	Frequency Domain Decomposition
FE	Finite Element
FEM	Finite Element Model
FVA	Forced Vibration Analysis
GPS	Global Positioning System
IRF	Impulse Response Function
LTHA	Linear Time History Analysis
LTI	Linear Time Invariant
MAC	Modal Assurance Criterion
MDOF	Multi Degree of Freedom
NTHA	Nonlinear Time History Analysis
OMA	Operational Modal Analysis
OMAX	Operational Modal Analysis with eXogenous Inputs
PD	Public Domain
PDF	Probability Distribution Function
PGA	Peak Ground Acceleration
PSD	Power Spectral Density
SDOF	Single Degree of Freedom
SHM	Structural Health Monitoring
SVD	Singular Value Decomposition
SVL	Singular Value Line

1. INTRODUCTION

1.1. Structural Health Monitoring Overview

As new strong shaking events take place, our understanding on how actual structures respond to real quakes, and as more surveys are carried out, our earthquake hazard maps change. Correspondingly, the building codes and the vigor with which they are overseen, change as well. However, existing structures can not reflect to these changes. And their safety needs to be reevaluated in the light of the new knowledge.

New and old, all structures are transformed into a Finite Element Model (FEM) to mimic the actual structure for these assessments to be made. The degree of success of the FEM to mimic the actual structure varies and it is inevitably limited. This forms a major contributor of error in any assessment more detailed than a visual check.

It is customary to employ tests such as the concrete compression tests to at least increase confidence in fundamental unknowns. But, without Structural Health Monitoring (SHM) there is no way of actually knowing the *real* modal parameters and thus, dynamic characteristics of the structure. Because, structural health monitoring utilizes the vibrational data (acceleration, velocity or displacement) taken from the real world structure.

This enables us to be able to measure how far off, thus how dependable our FEM is, and presents us with the opportunity to improve our FEM to better approximate the actual structure. Through which process, namely the model updating, we can enhance our FEM to a level such that it can detect the unseen damages to a structure, which would be missed during a visual check.

As can be seen from Figure 1.1, Structural Health Monitoring is divided into distinct segments. These include, planning the tests, obtaining the vibrational data, processing this data by system identification algorithms to obtain modal parameters,

and model updating of the FEM for structural assessments to be performed.

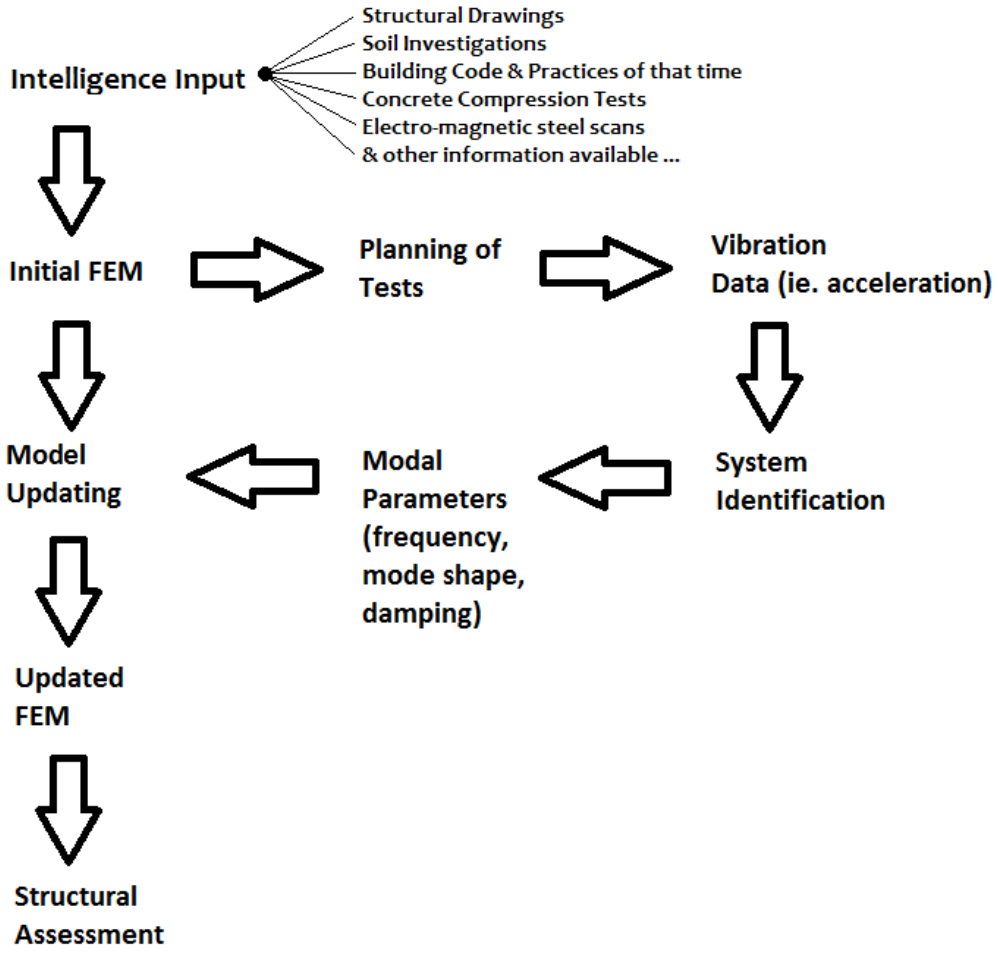

Figure 1.1. Structural Health Monitoring Procedure.

Going through from the start of the flow chart to its end, firstly it is generally the case that for old structures the structural drawings necessary to make the initial FEM are either missing or incomplete. Furthermore, as structure gets older, it is more likely that the building code of that time was not closely applied. The effects of corrosion, creep, shrinkage and fatigue can vary widely from structure to structure and there may be additional damage from various loadings. Thus, the initial FEM inaccurately represents the actual structure.

The tests are planned from this initial FEM, to try and validate the modes of vibration. Sensors, generally accelerometers in civil engineering applications, are allo-

cated for capturing the highest amplitude motions in the expected modes. Strategic placement of the sensors should be accounting for the fact that the expected modes and the actual modes are different, this may require more than one sensor *configuration* to be utilized.

Modal testing is divided into two major types, forced vibration testing and ambient vibration testing. In forced vibration testing, the structure tested is subjected to a quantified and measured loading input such as loadings produced by an eccentric mass shaker or from release of a known mass attached to a cable. Whether a load of a controlled frequency or an impact load is applied, the loading is known and the accelerometers or other types of vibration sensors record the structure's response to these loads.

In ambient vibration testing, also known as Operational Modal Analysis (OMA), the structure is not loaded in a controlled manner but by the existing low amplitude vibrations, ambient vibrations, in everyday-operational environment of the structure. Since the properties of the structure, namely its transfer function is to be deduced from the input (loading), output (vibrations) relationship of the structure, there is a need for an assumption of the statistical nature of the input. This requires the output to be interpreted in terms of random data of a given type (ergodic, stationary, etc. and generally *Gaussian White Noise with zero mean* [1]).

Depending on the type of vibration test to be applied i.e. forced or ambient, associated equipment is placed and the data are taken. This raw data are then processed by signal processing techniques to account for noise, leakage, spilling, aliasing and jumps in the data. This processed data are at this stage ready to be implemented in a system identification algorithm. There are many choices for such algorithms and some depend on the type of the vibration test that has been applied. These algorithms output the modal parameters of the structure such as its modal frequencies, mode shapes and the damping ratios of each mode.

Using the modal parameters obtained, the initial FEM undergoes a model up-

dating process to yield the most plausible set of FEMs to mimic the actual structure's behavior. Then these set of FEMs are used to evaluate the structural safety of the actual structure in computer simulations.

On more inclusive terms, SHM is defined as "The process of implementing a damage identification strategy for aerospace, civil and mechanical engineering infrastructure" and fundamentally as a statistical pattern recognition problem. [2]. Although, not as developed as its rotating machinery counterpart, namely, *condition monitoring*, SHM is commercialized in some civil engineering uses, especially in bridge applications, due to regulatory requirements in Asian countries that require the construction companies to regularly assess the health of the structure.

There are five interrelated disciplines that are similar in nature, it is thought that their definition and fields they apply should be given here to avoid representing SHM in isolation, since developments in one of the following could lead immediate corresponding advances in the others. Below are the four of the five disciplines, where the fifth is SHM.

(i) *Condition Monitoring* is direct SHM counterpart for rotating machinery.
(ii) *Non-Destructive Evaluation* is the term generally used for identification of damage severity after it has been localized. Typical applications include pressure vessels and rails.
(iii) *Statistical Process Control* is concerned with changes in a process, rather than a structure, that are identified via various kinds of sensors.
(iv) *Damage Prognosis* is concerned with estimating the remaining useful life of a structure, after damage has been found.

The fifth discipline and the focus in this study is SHM, which emphasizes more on the global structural character and is mainly applied for civil and aerospace structures. Through vast amount of research in the literature the following fundamental axioms on SHM can be concluded [3].

(i) All materials have inherent flaws

(ii) Assessment of damage requires a comparison between two system states

(iii) Type and severity of damage (not mandatory for existence and location) can be identified in a supervised learning mode, which requires an undamaged and damaged state to be known.

(iv) Without intelligent feature extraction, the more sensitive a measurement to damage, the more sensitive it is to changing operational environments.

(v) The length and time scales associated with damage dictate SHM sensing system.

(vi) Trade off for noise cancellation and damage sensitivity exists for any algorithm.

(vii) The size of the damage that can be detected from changes in system dynamics is inversely proportional to the frequency range of excitation.

Some of the above axioms are self-explanatory like all materials having inherent flaws, others might benefit further elaboration. Axiom five in civil engineering terms can be translated as a case example by trying to assess the loss of rigidity of a pre-stressed bridge due to cable relaxation over time to be able to replace the cables when necessary, the time scale involved requires years for substantial relaxation to occur, therefore either intermittent but regular, or continuous monitoring of the structure for this period is required, since the loss of stiffness due to cable relaxation would need to be separated from any other type of stiffness loss occurring during this period (axiom three is in effect also for this example).

Axioms six and seven relate to the understanding that as the size of the damage gets smaller, the modes majorly effected happens to be modes of higher order, therefore importance of extracting information involving higher frequencies, elevates. This condition in turn reverts back to axiom five about the spatial consideration in monitoring. Since, quality assured monitoring of higher modes generally involves more densely spaced monitoring equipment. This can easily be intuitively understood by simple comparison between the frequency ranges, spatial configurations and sizes of damage involved in applications of aerospace or mechanical engineering versus applications of civil engineering. It is noteworthy to realize the statement in axiom four is then

self-compensated by the fact that mechanical and aerospace engineering structures are of smaller sizes to allow more stringent testing to be applied under thoroughly controllable environments. An example study for finding localized damage in civil engineering structures can be found in [4].

In general terms, most often the concern for civil engineering structures is the ability to withstand major events such as earthquakes or blast and impact loads, thus, the overall integrity of the structure is of main concern. Therefore, focusing the attention of the testing to first few modes in most cases is natural and common. This allows civil engineering structures to be economically assessed by SHM with a comparably low number of observation points on the structure.

1.2. Literature Review

One of the problems SHM might help solve, is the validation of integrity in aging bridges. Due to their importance in economic and social links they provide, it is a common practice to monitor the condition of bridges periodically, with or without the utilization of SHM. These checks are conventionally made by visual measures. The inadequacy of the conventional approach is realized in many bridge failures throughout the world, including Turkey, in events such as 6 April 2012 Çaycuma incident, where 15 people have died.

Accordingly, several studies concerning bridges have been and are being made in SHM. Studies on bridges show a wide scatter of different structural configurations that reflect various available approaches in bridge design. In [5] a Turkish post-tensioned highway bridge with friction pendulum isolators is tested and its FEM is updated to yield the effectiveness of the friction pendulum isolators in reducing the seismic effects, using the 1992 Erzincan earthquake data. In [6], the then 120 years old Paderno bridge, which is a typical example of a steel arch bridge of the late 19th century, with inward bent arch ribs and masonry piers is tested. Consistently with ones expectations on corrosion's effect on steel, the results show the difference in strength of the two sides of the steel structure, facing upstream and downstream of the river it passes over. In [7],

it is shown that the condition of cables in a cable-stayed bridge can be recognized from parameters that are derived from the frequency and damping values obtained from the cables. These examples can be considered as proof for the effectiveness of SHM to yield results that are not obtainable conventionally, but they can also be seen to stress the possible requirement of distinct expertise in specific structural configurations for these applications to be successful.

This is perhaps more valid for cable-stayed and suspension bridges, where pure cable modes and variable wind speeds during testing, pose problems to be addressed for reliable estimation of modal parameters, especially damping. Same is true for structures that utilize cables, such as suspended roofs as in [8], where researchers acknowledge the need for further improvements for determining the modal damping ratios. There are numerous studies on reliable identification of damping, yet damping ratio stays as one of the most elusive of the parameters to be extracted.

Along with advances made in system identification for modal parameter extraction, a parallel development can be observed in the technology behind sensory equipment. Capability of maintaining high sensitivity in low amplitude disturbances, especially in the case of force-balance type accelerometers, which are comparatively cheap in relation to their piezoelectric and other sensory counterparts, has allowed the SHM tests that do not utilize expensive artificial input generators, namely OMA to become more adequate. This in turn have shifted the attention from Forced Vibration Analysis (FVA) to OMA, in system identification algorithms being developed, such as the Frequency Domain Decomposition (FDD) method, which has become one of the most frequently used algorithms.

In this regard, the advances in the sensor technologies directly effect the productivity obtainable from SHM. Exciting new technologies continue to emerge, such as laser doppler vibrometers that are time synchronized via Global Positioning System (GPS). But, perhaps more importantly new algorithms are developed to make some other mature technologies, that are previously uncorrelated with SHM, become cheap and effective SHM sensory equipment. One such attempt involves regular digital cam-

eras and wireless routers that are familiar in our daily lives. This set up, for which detailed description is given in [9], utilizes image processing software to translate visual vibrations recorded via cameras into numerical data series. The time synchronization is achieved by a master computer gauging the time delays in the communication to and from the sub-systems through a wireless router (TCP/IP connection), prior to the collection of data. Each sub-system is composed of a camera and a dedicated computer which runs the image processing softwares. The sub-system computer also manages the brightness and contrast settings of the camera to account for the change in the lighting conditions throughout testing. Current applications use a dotted target mark to be tracked by the image processing software. Each sub-system can monitor one such target (degree of freedom) and send the calculated displacement values to the master computer. One could expect as the image processing softwares continue to improve, a single sub-system might be able to monitor every pixel sized degree of freedom in its camera lens view. Such a precision could make assessment of even local damage type and severity, an automated work.

Regardless of the above mentioned high spatial resolutions in data collection that might be possible in the future, the analytical models of a structure has long been expected to perform at high spatial resolutions to exhibit a realistic approximation of motion of the real structure, with increasing processing power of the PCs in the past decades. Furthermore, the level of detail in FEMs required to solve inverse problem of SHM is far above the level of detail one can settle for in a structural design process, [10]. There are several examples of highly detailed models being used to obtain successful SHM results. In [11] IASC-ASCE structural health monitoring benchmark steel structure is tested with OMA and many consistent damage patterns with the test structure's damage profile has been found. In [12] a landslide induced damage on the slab system of a building is analyzed. In axioms given in the section 1.1 we have mentioned that, although locating damage does not require a prior system state information, identifying damage severity does. In [12] the undamaged portions of the slabs have been successfully used as a plausible prior state for the damaged slab. This goes to show that SHM applications are not bound for earthquake hazard applications and global assessments only, and they can be successfully implemented in other damage

scenarios including very localized ones.

However, the focus of the bulk of the research on SHM in civil engineering and the focus of this thesis as well, is the utilization towards global health assessment and more precisely earthquake hazard mitigation. For any city that falls within zones of moderate to high seismic hazard, the task of reducing the expected losses in a strong earthquake is a challenging one. It is not economical, for the most part, to examine all of the building stock in great detail. Some researchers and institutions have therefore adopted a more categorizational approach towards the city wide or even the country wide situation [13–15]. These are accompanied by studies on the extent of damage detection capabilities in rather controlled environments, [16], and structural configuration specific studies designed to enhance the approach towards the design of specific kinds of structures, [17].

The holistic approach undertaken as described above requires a complementary assessment procedure for massive numbers of structures in a city. In [18, 19] the issue of checking the safety of large amounts of structures, economically, is addressed for low to medium seismic hazard regions. In the proposed assessment approach, buildings higher than 5 stories are modeled as Timoshenko beams, and these simple models are updated with modal parameters extracted from ambient vibration tests. This updated model is used to determine the acceleration level that correspond to a *seismic integrity threshold*, [19]. This threshold is defined as the acceleration level corresponding to the tensile failure in the reinforced concrete members of the idealized Timoshenko beam model.

The seismic integrity threshold introduced above is intended for low to medium seismic hazard regions. For high seismic hazard locations however, the method is not useful, and more costly but detailed assessment methodologies are somewhat inevitable. Although, there are no SHM directives in the current Turkish seismic code, [20], the requirements for undertaking earthquake performance assessments for existing buildings in chapter 7 of [20], supplies an understanding of the relative detail of the approach deemed satisfactory by the Turkish government for high seismicity zones. The re-

quirements for stripping the reinforced concrete members off of their clear covers for examination of the reinforcement, testing concrete core examples for strength and the investigation of the soil beneath the structure, are essential for a reliable assessment of structures in high seismicity zones, regardless of the utilization of SHM techniques. Therefore, it shall be noted here that SHM is not a way out of test and analysis commitments in the current assessment methodology, but it is a new source of information for model generation and damage detection, stemming from the *actual* dynamic characteristics of the structure, that are otherwise not attainable.

1.3. Motivation

Turkey is a country with many active faults. Marmara region hosts a population of $22,000,000$ of which $13,500,000$ reside in İstanbul province. The city, sitting on the western side of the North-Anatolian fault, a location expected to host major seismic events [21], is under severe seismic hazard. This is the same fault line that generated strong earthquakes like 1999 İzmit and 1999 Düzce earthquakes with tens of thousands in casualties.

Alarmingly, the structural safety of the majority of buildings in İstanbul is of question. However, there are active movements towards rehabilitation, reconstruction and re-urbanization of the densely populated city.

OMA based SHM can be a great asset under these circumstances, both for prioritization of the renewal projects and for the reliability of assessments. It is also possible to guide the retrofitting projects with damage detection capabilities. SHM and particularly for its ease of implementation and low cost, OMA can become one additional requirement for payment acceptation terms in the construction projects to be made in place of demolished structures. This could also enable a basis for damage prognosis in post-earthquake evaluations. These form a brief introduction to the possibilities of utilizations of SHM for İstanbul. But, such an attempt needs to be able to confront difficulties in SHM of the typical aging reinforced concrete structures in the city, that are closely packed, in lack of structural drawings and soil investigations and built ac-

cording to much older design codes with insufficient ductility issues. These difficulties need to be confronted for a massive number of structures in a systematic, reliable and cost-efficient fashion within an acceptable amount of time.

With this motivation, the ETA-B building in Boğaziçi University north campus, a building representative of the building practices of the time when the 1975 design code, [22] was in jurisdiction, is assessed with SHM to provide an exemplary evaluation of similar structures.

1.4. Scope

The mathematical background for SHM is diverse, both the signal processing and the system identification relies heavily on an array of different topics. Therefore, mathematical self containment is aimed at in this thesis. For this purpose Appendix A is formed. It includes the formulation of Fourier transform from simple, complex algebra and trigonometry identities, and extends to stochastic processes briefly in a way to include theorems like the cross-correlation theorem necessary for derivations required for the Enhanced Frequency Domain Decomposition (EFDD) method. Therefore, it is a mathematical introduction to the signal processing in Appendix B and system identification in Chapter 2.

Chapter 2 starts with structural dynamics and builds up to response to random vibrations via Appendix A, and then continues into the system identification theory and eventually the EFDD method in detail, which is the method of identification used in the case study. This chapter also includes an overview of the model updating process.

Chapter 3 introduces the EFDD algorithm developed in this thesis for the identification process and the application of this code to the case study, the ETA-B building. Chapter 4 includes an introduction for the proper modelling of structures for the purpose of SHM, which is much more detailed in nature when compared to regular design purpose models. It continues to describe the FEM developed for ETA-B building in detail and its updating process via the OMA results.

In Chapter 3, along with an overview on OMA, the developed EFDD code is introduced and its application to ETA-B building is presented. Chapter 4 starts with an overview of the general FEM development considerations for SHM, it describes how the FEM of ETA-B is formed and then updated.

Chapter 5 starts with an overview on modern performance based earthquake assessment techniques, it then shows the Linear Time History Analysis (LTHA) applied to the models, following the description on how the earthquakes were selected. Finally, Chapter 6 includes the conclusions and recommendations as the overall result of this study. It should be noted that, the overview and the theory sections in this thesis are not unbiased, and are tailored to fit the needs of elaboration required for the proceeding chapters of the study, and can not form a complete picture of the highly diverse topics discussed.

2. THEORY OF STRUCTURAL HEALTH MONITORING

2.1. Random Vibrations

2.1.1. Structural Dynamics

In ambient vibration testing, OMA, the input-loading to the structure is in the form of *random vibrations*. As a preface to system identification under OMA, it is needed to first set up structural dynamics formulations and the transfer function. Next, it is necessary to discover the relationship of this transfer function to Power Spectral Density (PSD) of the response to random vibrations. Because, our algorithms are dependent on extracting information from this PSD.

$$m\ddot{u}(t) + c\dot{u}(t) + ku(t) = F(t) \tag{2.1}$$

Equation 2.1 is the equation of motion of a lumped, single degree of freedom mass, that acts linearly in k and is viscously damped. If we take Fourier integral transform of both sides of this equation and make some arrangements, we obtain the following.

$$-mw^2u(w) + icwu(w) + ku(w) = F(w) \tag{2.2}$$

$$u(w) = F(w) \times \frac{1}{k - mw^2 + icw} \tag{2.3}$$

$$u(w) = F(w) \times H(w) \tag{2.4}$$

where,

$$H(w) = \frac{1}{k - mw^2 + icw} = \frac{u(w)}{F(w)} \tag{2.5}$$

is the *transfer function* for this single degree of freedom system. The Fourier pair of the transfer function $h(t)$ is known as the *impulse response function*.

$$h(t) = \frac{1}{2\pi} \int_{-\infty}^{\infty} H(w) e^{iwt} \, \mathrm{d}w \tag{2.6}$$

$$h(t) = \begin{cases} \frac{e^{-\xi w_n t}}{m w_d} sin(w_d t) & , t \geq 0 \\ 0 & , t < 0 \end{cases} \tag{2.7}$$

where,

$$w_n = \sqrt{\frac{k}{m}}, \text{ Natural frequency in rad-Hz} \tag{2.8}$$

$$\xi = \frac{c}{2 m w_n}, \text{ Damping ratio} \tag{2.9}$$

$$w_d = w_n \sqrt{1 - \xi^2}, \text{ Damped natural frequency in rad-Hz} \tag{2.10}$$

As shown in Appendix A.1 Equation A.43, a multiplication in frequency space $u(w) = H(w)F(w)$ is a convolution in time space $u = h * F$. Then we have for $u(t)$ the formula known as the *Duhamel's integral*.

$$u(t) = \int_{-\infty}^{\infty} F(\tau) h(t - \tau) \, \mathrm{d}\tau \tag{2.11}$$

$$u(t) = \frac{1}{m w_d} \int_{0}^{t} F(\tau) e^{-\xi w_n (t-\tau)} sin(w_d (t - \tau)) \, \mathrm{d}\tau \tag{2.12}$$

Same conclusion can also be reached via factoring $F(t)$ into a series of impulses (which is same as $f = f * \delta$) and then superimposing the responses to individual impulses for $u(t)$ up to t. From Equation 2.12 $\dot{u}(t)$ and $\ddot{u}(t)$ can be calculated by differentiation.

For multi degree of freedom systems, Equation 2.1 becomes,

$$[m]\{\ddot{u}(t)\} + [c]\{\dot{u}(t)\} + [k]\{u(t)\} = \{F(t)\} \tag{2.13}$$

Where $[m], [c], [k]$ are, $N_{dof} \times N_{dof}$ matrices, $\{\ddot{u}(t)\}, \{\dot{u}(t)\}, \{u(t)\}, \{F(t)\}$ are N_{dof} length vectors dependent on time, N_{dof} is the number of dynamic degrees of freedom. We will assume a diagonal mass matrix and no rigid body translation in the remaining sections with Equation 2.13.

If we introduce the *modal decomposition* of $\{u(t)\}$ as,

$$\{u(t)\} = [\Phi]\{q(t)\} \tag{2.14}$$

Where $[\Phi]$ is the modal matrix (or mode shape matrix) and $\{q(t)\}$ is the modal motion vector composed of independent-uncoupled single degree of freedom motions $q_i(t) \quad for \quad i = 1, 2..., N_{dof}$. $\{\ddot{u}(t)\}, \{\dot{u}(t)\}$ follows the same decomposition with $\{\ddot{q}(t)\}, \{\dot{q}(t)\}$. $[\Phi]$ is found from the *eigenvalue problem* below.

$$w_n^2[m]\{\phi_n\} = [k]\{\phi_n\} \quad n = 1, 2, ..., N_{dof} \tag{2.15}$$

Which is reached from Equation 2.13 with $[c] = 0$, $\{F(t)\} = \{0\}$ and substituting for $\{u(t)\}$ and $\{\ddot{u}(t)\}$ according to Equation 2.14 through, $\ddot{q}_i(t) = -w_i^2 q_i(t)$ $w_i = w_n$ at $i = n$, for an undamped single degree of freedom system. (which can be shown from Equation 2.12 with $c = 0$)

By solving this eigenvalue problem we obtain w_n natural frequencies and ϕ_n mode shape vectors which form $[\Phi]$ by becoming nth column in $[\Phi]$. For the calculations below $[\Phi]$ will stand for *mass normalized* $[\Phi]$, such that,

$$[\Phi]^{-1} = [\Phi]^T[m] \tag{2.16}$$

Decomposing damped Equation 2.13 with Equation 2.14 and multiplying both sides with $[\Phi]^T$ from the left, we obtain,

$$[\Phi]^T[m][\Phi]\{\ddot{q}(t)\} + [\Phi]^T[c][\Phi]\{\dot{q}(t)\} + [\Phi]^T[k][\Phi]\{q(t)\} = [\Phi]^T\{F(t)\} \tag{2.17}$$

Since the $[\Phi]$ is mass normalized, $[\Phi]^T[m][\Phi] = [I]$ and from Equation 2.15 $[\Phi]^T[k][\Phi] = [\Omega]$ where $[\Omega]$ is the diagonal matrix of w_i^2, $i = 1, 2, ..., N_{dof}$.

$$[I]\{\ddot{q}(t)\} + [\Phi]^T[c][\Phi]\{\dot{q}(t)\} + [\Omega]\{q(t)\} = [\Phi]^T\{F(t)\} \tag{2.18}$$

Let,

$$[C] = [\Phi]^T[c][\Phi] and \{Q(t)\} = [\Phi]^T\{F(t)\} \tag{2.19}$$

Assuming $[c]$ is a linear combination of $[m]$ and $[k]$ as in *proportional damping*, so that $[C]$ is a diagonal matrix.

$$[I]\{\ddot{q}(t)\} + [C]\{\dot{q}(t)\} + [\Omega]\{q(t)\} = \{Q(t)\} \tag{2.20}$$

This is a decomposition into independent single degree of freedom systems $q_i(t)$, $i = 1, 2, ..., N_{dof}$, from the definition of damping ratio in single degree of freedom systems, we get the *modal* damping ratios as $\xi_i = \frac{C_{ii}}{2w_i}$ since $I_{ii} = 1$ which would stand for mass for these single degree of freedom equations (The first subscript in matrix variables above is the row index and the second is the column index.).

$$\ddot{q}_i(t) + 2\xi_i w_i \dot{q}_i(t) + w_i^2 q_i(t) = Q_i(t) \tag{2.21}$$

For each of such independent single degree of freedom systems the transfer function is in the form in Equation 2.5. To distinguish it from the multi degree of freedom transfer function to be derived here, let us denote this single degree of freedom transfer function

as $H(w)_q$.

$$H(w)_q = \frac{1}{w_i^2 - w^2 + i2\xi_i w_i w} \tag{2.22}$$

Then we can derive the multi degree of freedom transfer function as the following.

$$Q_i(t) = \sum_\alpha \phi_{i\alpha} F_\alpha(t) \tag{2.23}$$

$$u_\alpha(t) = \sum_i \phi_{\alpha i} q_i(t) \tag{2.24}$$

$$Q_i(w) = \sum_\alpha \phi_{i\alpha} F_\alpha(w) \tag{2.25}$$

$$u_\alpha(w) = \sum_i \phi_{\alpha i} q_i(w) \tag{2.26}$$

since,

$$q_i(w) = H(w)_q Q_i(w) \tag{2.27}$$

$$u_\alpha(w) = \sum_i \phi_{\alpha i} \frac{\sum_\beta \phi_{i\beta} F_\beta(w)}{w_i^2 - w^2 + i2\xi_i w_i w} \tag{2.28}$$

$$u_\alpha(w) = \sum_i \sum_\beta \frac{\phi_{\alpha i}\phi_{i\beta} F_\beta(w)}{w_i^2 - w^2 + i2\xi_i w_i w} \tag{2.29}$$

$$u_\alpha(w) = \sum_\beta H_{\alpha\beta}(w) F_\beta(w) \quad \equiv \quad \{u(w)\} = [H(w)]\{F(w)\} \tag{2.30}$$

where,

$$H_{\alpha\beta}(w) = \sum_i \frac{\phi_{\alpha i}\phi_{i\beta}}{w_i^2 - w^2 + i2\xi_i w_i w} \tag{2.31}$$

Equation 2.31 is the transfer function relating the β coordinate applied forcing function to the α coordinate response, and forms the αth row βth column entry in $[H(w)]$.

2.1.2. Response to Random Vibrations

For multi degree of freedom systems $u_1(t), u_2(t), ...u_{N_{dof}}(t)$, If $R_{uu}(\tau)$ is the correlation matrix of responses, then

$$[R_{uu}(\tau)]_{ij} = \int_{-\infty}^{\infty} u_i(t)u_j(t+\tau)\ \mathrm{d}t \tag{2.32}$$

If we take the Fourier transform of $R_{uu}(\tau)$ matrix, we obtain $S_{uu}(w)$ power spectral density matrix of the responses. By cross-correlation theorem Equation A.48, we have,

$$[S_{uu}(w)] = \left\{ \begin{array}{c} \overline{u_1(w)} \\ \overline{u_2(w)} \\ \vdots \\ \overline{u_{N_{dof}}(w)} \end{array} \right\} \times [u_1(w)u_2(w)\dots u_{N_{dof}}(w)] \tag{2.33}$$

If we expand with Equation 2.30,

$$\begin{aligned} [S_{uu}(w)] &= \overline{([H(w)]\{F(w)\})} \times ([H(w)]\{F(w)\})^T \\ &= \overline{[H(w)]\{F(w)\}}\{F(w)\}^T[H(w)]^T \\ &= \overline{[H(w)]}[S_{FF}(w)][H(w)]^T \end{aligned} \tag{2.34}$$

(where overbar stands for complex conjugate.)

$$[S_{uu}(w)] = \overline{[H(w)]}[S_{FF}(w)][H(w)]^T \tag{2.35}$$

Equation 2.35 will form the starting point of our system identification algorithm in enhanced frequency domain decomposition technique. Equation 2.35 can be reduced

to single degree of freedom case as,

$$S_{uu}(w) = |H(w)|^2 S_{FF}(w) \tag{2.36}$$

Although not proven here, the two other important relationships in the following equations are also true for single degree of freedom systems, [23] (and they can be expanded to multi degree of freedom systems as well).

$$S_{Fu}(w) = H(w) S_{FF}(w) \tag{2.37}$$

$$S_{uu}(w) = |H(w)|^2 S_{uF}(w) \tag{2.38}$$

2.2. System Identification

2.2.1. Overview

As mentioned earlier, the two possible scenarios for modal testing involves supplying an input to the structure or not, FVA and OMA respectively (and Operational Modal Analysis with eXogenous Inputs, OMAX as a hybrid method). With the advent of highly sensitive transducers, the identification of output-only case has gained critical importance due to the high costs associated with loading civil engineering structures in a controlled manner through heavy and costly machinery. Although many developed and widely accepted FVA methods exist for identification, only the output-only case is discussed here for its relevance to the study here in.

However, some of the input-output based methods can be extended into output-only case through appropriate adjustments [1].

The output only identification methods can be subdivided into time domain methods which are parametric and frequency domain methods that are not.

Time domain methods involve setting up an appropriate mathematical model to idealize the dynamic behavior of the structure. State-space stochastic, ARMAV and ARV models are usually used [1]. Then the parameters are solved for to obtain modal unknowns with closest fit possible to experimental data. Time domain methods tend to provide the best results for the cases where there exist a large number of modes, and they can be *completely automated* in terms of obtaining the modal parameters [1].

Frequency domain methods such as FDD and EFDD that are discussed in detail in the following section, are non-parametric methods. They are easy to understand and follow since, they are more graphical [24]. They base the identification algorithm on an assumption of the unknown input being *Gaussian White Noise with zero mean*, and this occasionally cause computational modes to manifest [1].

Specifically speaking for FDD and EFDD, they involve engineer's input on the software at different stages and they are less automated than time domain methods, such cases involve, deciding whether or not a mode has been found by checking the consistency of the Modal Assurance Criterion (MAC) values for the obtained mode shape around the peak frequency, deciding whether or not a harmonic is in play on the singular value lines, assuring the weaker mode's mode shape is not biased (orthogonal with dominant one) whenever two modes are close and deciding to take another singular value line for evaluation, if any given two modes are nearly repeated. However, they make it possible to get a feeling for the structure under consideration. It would be possible to obtain both an understanding of the structure and ease of prolonged monitoring with the use of time domain and frequency domain methods in combination. It should also be noted that fully automated frequency domain algorithms are gaining ground such as the LEONIDA algorithm for fully automated OMA testing [25, 26].

2.2.2. Enhanced Frequency Domain Decomposition Technique

EFDD technique is a derivative of FDD method. In this section FDD is outlined with its theory and interpretations and where appropriate the EFDD's difference is introduced.

In order to be successful, FDD requires some conditions to be met in OMA [24],

- Broad band excitation (white noise as best case)
- Light damping
- Orthogonal mode shapes (especially for close modes)

The third requirement above needs further elaboration, since one eigenvalue matches one eigenvector in Equation 2.15. It is expected that all mode shapes are orthogonal by definition. But, these vectors consist of infinitely many degrees of freedom in reality, the third condition states that we should have observed degrees of freedom in adequate number and in well chosen locations to differentiate any close modes that are of interest to us (i.e. structurally important for earthquake response).

We can follow the theory from Equations 2.22, 2.31 and 2.35 by the assumption of independent white noises at each input loading [24]. Let,

$$\begin{aligned}
\tilde{\beta} \geq \beta \geq 1 \quad &, \text{index of applied force's degree of freedom} \\
\tilde{\alpha} \geq \alpha \geq 1 \quad &, \text{index of measured response's degree of freedom} \\
n \geq i \geq 1 \quad &, \text{mode number}
\end{aligned}$$

By Equation 2.22 and 2.31,

$$H_{\alpha\beta}(w) = \sum_{i=1}^{i=n} \phi_{\alpha i} H(w)_{q_i} \phi_{i\beta} \quad \equiv \quad [H(w)]_{\tilde{\alpha}\tilde{\beta}} = [\Phi]_{\tilde{\alpha}n} [H(w)_q]_{nn} [\Phi]^T_{n\tilde{\beta}} \tag{2.39}$$

Where, $[H(w)_q]_{nn}$ is a diagonal matrix of modal motions at w, and the subscripts below matrices denote number of rows and columns each matrix has.

Applying Equation 2.39 and $[S_{FF}(w)] = [C]$ where $[C]$ is a constant diagonal matrix for all w to facilitate independent white noise assumption to Equation 2.35,

$$[S_{uu}(w)]_{\tilde{\alpha}\tilde{\alpha}} = [\Phi]_{\tilde{\alpha}n} \overline{[H(w)_q]}_{nn} [\Phi]^T_{n\tilde{\beta}} [C]_{\tilde{\beta}\tilde{\beta}} [\Phi]_{\tilde{\beta}n} [H(w)_q]^T_{nn} [\Phi]^T_{n\tilde{\alpha}} \tag{2.40}$$

Since $[C]$ is diagonal and $[\Phi]$ has $[\Phi]^T = [\Phi]^{-1}$ orthogonality property,

$$[\Phi]^T_{n\tilde{\beta}}[C]_{\tilde{\beta}\tilde{\beta}}[\Phi]_{\tilde{\beta}n} = [C']_{nn} \tag{2.41}$$

Where $[C']_{nn}$ is also a diagonal constant matrix with modified numbers and size. With above statements $[S_{uu}(w)]$ becomes,

$$[S_{uu}(w)]_{\tilde{\alpha}\tilde{\alpha}} = [\Phi]_{\tilde{\alpha}n}\overline{[H(w)_q]}_{nn}[C']_{nn}[H(w)_q]^T_{nn}[\Phi]^T_{n\tilde{\alpha}} \tag{2.42}$$

Where $\overline{[H(w)_q]}$, $[C']$ and $[H(w)_q]^T$ are all diagonal,

$$\overline{[H(w)_q]}_{nn}[C']_{nn}[H(w)_q]^T_{nn} = [|H(w)_q|^2C']_{nn} \tag{2.43}$$

$[|H(w)_q|^2C']_{nn}$, which is also a diagonal matrix, stands for $[|H(w)_q|^2]_{nn}$ with each diagonal multiplied with associated constant in $[C']$ for all w.

With all of the above, we obtain $[S_{uu}(w)]$ as,

$$[S_{uu}(w)]_{\tilde{\alpha}\tilde{\alpha}} = [\Phi]_{\tilde{\alpha}n}[|H(w)_q|^2C']_{nn}[\Phi]^T_{n\tilde{\alpha}} \tag{2.44}$$

It is important to note the meaning of the change in sizes of the $[\Phi]$ matrix in above calculations, in an ideal condition we would have $n = \tilde{\alpha} = \tilde{\beta}$ and they would equal to infinity. Although, $\tilde{\beta}$, the number of force application points and n, the number of existing modes, might go to infinity in their own accord, $\tilde{\alpha}$, the number of response degrees of freedom is limited by the number of *observable* response degrees of freedom due to finite number of sensory equipment. But, we also only need a limited number of n as well since we can distinguish the first few modes of the structure as most important in terms of their role in overall response, in this regard we can set $n = \tilde{\alpha}$ for a very close estimation.

$$[S_{uu}(w)]_{\tilde{\alpha}\tilde{\alpha}} = [\Phi]_{\tilde{\alpha}\tilde{\alpha}}[|H(w)_q|^2C']_{\tilde{\alpha}\tilde{\alpha}}[\Phi]^T_{\tilde{\alpha}\tilde{\alpha}} \tag{2.45}$$

This is a modal decomposition of $[S_{uu}(w)]$. The basic principle behind FDD is to estimate this decomposition through Singular Value Decomposition (SVD) at each w frequency.

SVD of a complex matrix is such that,

$$[A] = [U][\Sigma]\overline{[U]}^T \tag{2.46}$$

Where $[\Sigma]$ is real and diagonal, and $[U]$ is unitary ($[U]\overline{[U]}^T = [I]$). $[\Sigma]$ is composed of diagonal entries of singular values σ_i. The algorithms used for taking the SVD of a matrix can order these σ_i in decreasing order in the $[\Sigma]$, in the below discussions such a case is going to be assumed.

If we take SVD of $[S_{uu}(w)]$ at every w we obtain,

$$[S_{uu}(w)]_{\tilde{\alpha}\tilde{\alpha}} = [U(w)]_{\tilde{\alpha}\tilde{\alpha}}[\Sigma(w)]_{\tilde{\alpha}\tilde{\alpha}}\overline{[U(w)]}^T_{\tilde{\alpha}\tilde{\alpha}} \tag{2.47}$$

This is equivalent to Equation 2.45 with one important difference, since the σ_i are ordered by the SVD algorithm at each w, in order to construct the relevancy between Equation 2.45 and 2.47. We need to manipulate $[|H(w)_q|^2 C']$ and $[\Phi]$ to match the order of dominance of modes at that specific frequency.

If we collect all σ_i values for all w we can construct $\sigma_i(w)$ the *ith singular value line* and similarly we can construct $\{U'\}_i(w)$ the *ith singular vector*, where $\{U'\}_i$ stands for the ith column of $[U(w)]$ at that w.

In the neighborhood of some w_i the ith mode will be most dominant, thus $\sigma_1(w)$ will be an estimate of $|H(w)_{q_i}|^2 \times C'$ for that w neighborhood, and similarly, $\{U'\}_1(w)$ will be an estimate of ϕ_i, the ith mode shape. Outside of this w neighborhood, the ith mode will fall in dominance and it will progressively correspond to lower valued singular value lines. But it will be traceable through the MAC of its mode shape calculated with respect to each singular vector in $[U(w)]$. Therefore a complete $|H(w)_{q_i}|^2 \times C'_i$ picture

can be drawn in the spectrum for each mode. Each modal motion i is followed by an individual C_i' constant from our formulations, and since we will be extracting w_i and ξ_i values from this single degree of freedom spectrum C_i' value is of no importance, and we can normalize $|H(w)_{q_i}|^2 \times C_i'$ with its peak value, and from here on this normalized form is denoted as $|H(w)_{q_i}|^2$.

The key difference between FDD and EFDD is that EFDD uses a prescribed MAC limit for the portion of the singular value lines that can be included in the mode's auto spectra. Both methods look for peaks in the $\sigma_1(w)$ for indication of a mode and check MAC value consistency of $\{U'\}_1(w)$ in the w neighborhood for verification, but EFDD further sets a limit for the MAC value of $\{U'\}_1(w)$'s, outside this limit the singular value line is not associated with the mode in question.

If the two modes are exceptionally close, as if they are repeated modes, then the weaker mode can actually show its peak up in $\sigma_2(w)$ right below the dominant mode's peak in $\sigma_1(w)$. In case of such nearly repeated modes, the $\{U'\}_1(w)$ vector is still a good estimate of the dominant mode's mode shape, but if the mode shapes are not orthogonal, then the weaker mode's mode shape will be heavily biased [24].

If there is a harmonic in the record that we are interested in, it causes all or almost all singular value lines to rise at that harmonic's frequency, this allows for avoiding misidentifications of such harmonics as modes, through visual check [24].

Resonance frequencies and mode shapes of modes are extracted as described above. For damping ratio of these modes, one can either obtain them by half-power bandwidth methods from the peak of the mode or the $|H(w)_{q_i}|^2$ obtained for all w, (or until MAC limit is reached in case of EFDD), can be turned back to time domain by an inverse Fourier transform and the damping can be estimated from the Impulse Response Function (IRF) [24, 27].

2.3. Model Updating Approaches

There are different approaches when it comes to application of model updating. Main methods include Bayesian statistical framework [28] and sensitivity based approaches. An exemplary application of sensitivity based approach can be found in [29]. There is also applications revolving around inclusion of increasing detail to the FEM to mature the model by iterative means [1].

Bayesian model updating realizes that there can be more than one FEM to become the "updated" model, these set of models all conform (to a similar degree) to modal parameters extracted and there is no way of knowing which one is actually the representative of the real world structure. Therefore all of these models are considered as a set of possibilities (each equally likely or weighted) to be considered in the assessment of the structure.

There exist methods for locating damage and finding the type of damage in particular, that are not going to be addressed here. These shall involve a highly accurate FEM to begin with (of the undamaged condition), then the damage is tried to be found through fictitious damage applications to the model and comparing the results.

The following presents a summary of the description in [29] on sensitivity based model updating.

Sensitivity based model updating can be divided into three processes.

- Selection of reference data and extracted modal parameters
- Selection of parameters for updating
- Modal tuning based on selected parameters

Let,

R_e, vector of experimental response values
R_a, vector obtained by analytical response values
P_0, current parameters of the analytical model
P_u, updated parameters of the analytical model
S, sensitivity matrix

Where, the term response values is used generically and does not specifically mean displacement or acceleration values, but values obtain or extracted from associated model or experiment, whatever they might chosen to be. Then, the experimental and analytical (FEM based) response values and updating parameters relate to each other through the sensitivity matrix as,

$$R_e = R_a + S(P_u - P_0) \quad \equiv \quad \Delta R = S\Delta P \tag{2.48}$$

The ith row, jth column entry in the sensitivity matrix, S_{ij}, which gives the sensitivity of the ith element in R to unit change in jth element of P.

$$S_{ij} = \frac{\partial R_{a,i}}{\partial P_{u,j}} \quad \text{absolute sensitivity} \tag{2.49}$$

Where $i = 1, 2, ...n \quad j = 1, 2, ...m$ and n, m are number of response values and update parameters, respectively. Depending on the relative size of n and m, an updating problem can be determined ($n = m$), over-determined ($n > m$), or under-determined ($n < m$).

For all determinacy conditions Equation 2.48 can be solved, using a pseudo-inverse where required. $\Delta P = S^{+}\Delta R$, where the pseudo-inverse of sensitivity matrix

S^+ is given by,

$$S^+ = \begin{cases} S^{-1}, & n = m \\ (S^T S)^{-1} S^T, & n > m \\ S^T (S S^T)^{-1}, & n < m \end{cases} \tag{2.50}$$

Correlation analysis, is the study of resonance frequencies and mode shapes as *response values* for above equations. Then, R_e is extracted modal parameters such as w_n and phi_n and R_a is the same values obtained from the FEM.

Parameters to be updated are needed to be carefully selected by the magnitude of the effect they can impose on the analytical modal parameters and the number of parameters shall be carefully chosen. Beside these, the parameters must be constrained by upper and lower bounds so that the model does not converge to a physically meaningless state. An exemplary algorithm for solving this problem with boundary conditions is implemented and exemplified with trust region algorithm in [30].

Logically, if properly made different model updating techniques should converge to the same model or set of models. A detailed comparative study for connecting different model updating techniques and the resulting uncertainties can be found in [31].

3. MODAL TESTING OF ETA-B BUILDING

3.1. Operational Modal Analysis, a Critical Perspective

Operational modal analysis involves no expensive shaking equipment as opposed to forced vibration analysis. The issue of exciting structures gets more impractical as the size of the structure increases. Therefore operational modal analysis increase in importance for civil engineering structures.

Although less expensive, OMA has been shown to be a well suited solution for civil engineering structures where the results with forced vibration analysis are in good correlation [32].

In [32] it is shown that resonance frequencies, mode shapes and damping ratios obtained through OMA using FDD technique and FVA results are in full agreement for a two storey reinforced concrete test structure (Where damping comparison is made through a statistical approach with 90% confidence intervals).

It is important to note that in [32], the OMA has been realized by the excitation of a randomly walking person in the structure as one of the OMA cases. Although, the Gaussian white noise assumption is made in the OMA algorithms, the results are still in very good correlation with forced vibration results (Still, the excitation spectrum is required to be smooth enough even if not flat.).

OMA has some main drawbacks, firstly the mode shapes obtained are not scaled (i.e. mass normalized) since, not all degrees of freedom can be monitored. This issue is currently dealt by performing a second measurement after changing the mass of the structure by addition or removal of massive enough objects, if the mode shapes are desired to be scaled [33]. Alternatively, methods involving change in both mass and stiffness also exist such as in [34].

Second major drawback of OMA is that, operational excitation of the structure may be of narrow frequency band, this would lead to only a number of modes being extracted with high quality [33].

It is required to note here that the recent years has seen the development of the so called OMAX, *Operational Modal Analysis with eXogenous Inputs*, method as a hybrid solution between FVA and OMA. In which, the eXogenous input can be at levels of or lower than the amplitude of the operational forces. This in turn reduces the cost and size of the exciting equipment necessary. However exciting, the OMAX case is not considered in this study. A monte carlo simulation based comparison of OMA, OMAX and FVA cases can be found in [33].

3.2. An Overview of Code Developed for EFDD

EFDD method's algorithms are commercially available [35] and are used by many researchers. Short of such commercial code, an EFDD algorithm was developed for this study. Multi Degree of Freedom (MDOF) equation of motion solvers and signal processing codes to use in absence of a Fourier analyzer in the data logger are also developed. This section introduces some of the detail of these codes developed in the order of use in a typical OMA application.

All of the code developed for this thesis are intended to be put to public domain (PD) at a future date. Therefore, it is hoped that the descriptions given here along with the manuals supplied with the code, would enable further developments of the software.

As a first step and first possible improvement recommendation for developers the system lacks an automatic jump remover [36], which would be very useful. Currently the file Op_DATAPREP.m fixes data jumps via user input. Op_DATAPREP.m also removes trends from the data, it is observed by trial and error that the command "detrend" can remove trends without damaging the frequency content even if, it is overused. Therefore, for heavily trended data (i.e. due to a dangling data cable) it can

be recommended that a series of different orders of polynomials be removed by this command. After trend removal, Op_DATAPREP.m applies a low pass butterworth filter, preferred for its flat pass and stop band properties in OMA. It is also in this script that the voltage to g ratio of the specific accelerometers is accounted for.

WELCH.m file is written for the welching process of the above cleansed data, this file gives an easy to understand access to the capabilities involved in welching (i.e. padding zeros to increase data segment lengths etc.). But, it is not as fast as the built-in GNU Octave commands. When the performance becomes a problem, this can be fixed by changing the WELCH command in Op_SPECPREP.m file.

Op_SPECPREP.m outputs the response spectra and the SVLs up to the indicated cutting frequency in the filters (Curve fitting is currently applied for an artificial increase in frequency resolution with hopes for better damping estimation, however, this can easily be undone, if desired.). It is possible to add capability for detection and removal of "harmonics" from the spectra, currently there is a reminder for noting these possible harmonics down, when PSD is first plotted. Also, in this section two important parameters are requested, number of SVLs for mode detection (since, nearly repeated modes may cause the weaker mode to fall to the following Singular Value Line, SVL), and tolerance in SVL switching/jump down, which is used in the process described below.

After the SVD, the first SVL (and later the others if, number of SVLs for mode detection is entered as greater than 1.) is prompted repeatedly for each peak with calculated MAC values, in the neighborhood of the peak. The MAC values are plotted up to a local minima in MACs on the graph of the SVL. Figures 3.1 and 3.2 show a false mode with low MAC values (over an insignificant peak) and high MAC values on a true mode, respectively.

Currently, the code asks for validation of the realization of a mode, this can be improved to an automated detection state such as in LEONIDA, [25]. Where the obtained bell shape, is used as an approval criterion.

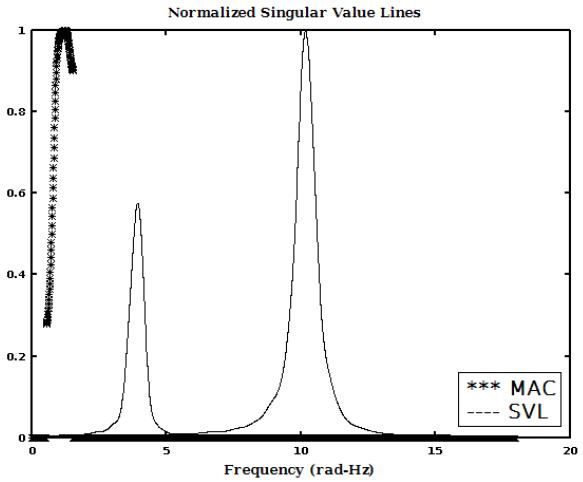

Figure 3.1. A False Mode Detected in Op_SDOFPREP.m.

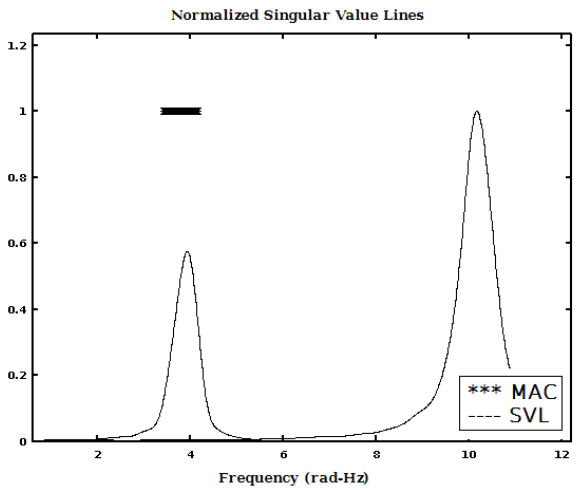

Figure 3.2. A Real Mode Detected in Op_SDOFPREP.m.

Op_SDOFPREP.m extracts the found modes up to limits of MAC values plotted. Then the previously obtained tolerance value is checked with the SVL below along with minimum allowed MAC value (EFDD criterion), until at least one of these conditions are false the algorithm jumps down to the below SVLs for the frequency range, terminating with filtering cut-off frequency.

Then Op_EXTRACT.m extracts the damping ratios from these Single Degree of Freedom (SDOF) auto-PSDs via inverse Fourier transform to obtain auto-correlation functions and then using logarithmic decrement (expfit built-in function is used which utilizes Prony equation, and the number of points for estimation is increased via prior curve spline to improve results). This process in particular needs further improvement, the utilization of a division by a triangular function in [8] is not entirely understood and thus, not implemented and the precision in [27] is not obtained with similar time segments, despite utilizing the mentioned 90%-20% limits on IRF.

Although not mentioned here, there are several sub-codes and procedures that are utilized directly or developed for complementary purposes. A general naming convention is followed for easy navigation of new users/developers.

- Nfoo.m are numerical manipulation codes
- foo.m are functions and/or Comprehensive Operations
- dev_foo.m are development stage codes
- T_foo.m are simulation codes for testing
- Op_foo.m are operational script codes

Where “foo” denotes the generic name for specific files. For simulation purposes, mdof.m gives exact solution of the differential equations in the time domain but is very slow. For testing purposes a mdof2.m function has been written which makes the solution in frequency domain and then returns it to time domain. While mdof2.m is much faster, its accuracy is lower. Its results catch up with the mdof.m within a reasonable data set, although abrupt changes (such as an impulse loading) in the forcing function of the equations may cause repetition of this catching up phenomenon. It has

been mainly used in the test and development stage of the EFDD code, to save time.

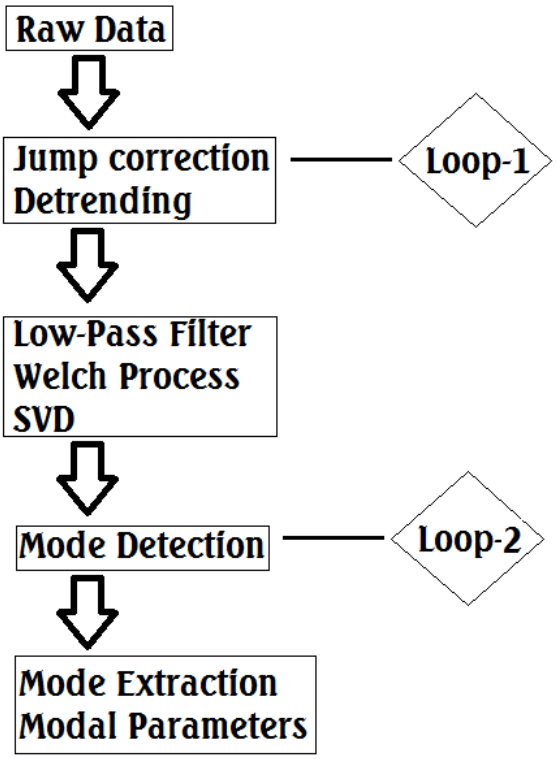

Figure 3.3. EFDD Algorithm Calculations Flow Chart.

Figure 3.3 shows the basic flow of computation, where loops 1 and 2 are dependent on user interactions as described previously.

3.3. Modal Testing of ETA-B Building

3.3.1. Structure Description

The subject of structural health monitoring in this study is the ETA-B building, located at Boğaziçi University's north campus, Figure 3.4.

Built according to the 1975 seismic code [22], ETA-B building is a 5 storey (excluding basement) reinforced concrete structure with a foundation of spread footings connected via grade beams. Basement perimeter walls and the staircase encasing throughout the height of the structure are the only sources of shear walls in the struc-

Figure 3.4. ETA-B Building and Its Location.

ture. The bottom of the footings (Level -1) are at level with the ground water table (Figure 3.5) and the beams at floor level (Level 0) show considerable visible damage due to water absorption and fall off of the concrete cover at certain locations due to swelling via excess moisture.

The structure was face to face with an approximately two and a half storeys high conference saloon, without any seismic precaution for pounding effects at the time of the testing. The close quarter construction of the two structures can be seen from the aftermath of the demolishing of the conference saloon in Figure 3.6.

As for slabs, the building has two types of floor systems, the upper 3 storeys are ribbed and below this, the slab system is formed by regular two-way slabs with perimeter beams.

The side views of ETA-B building can be found in Figure 3.8. As can be seen, the structure has a 3 storey expansion out of its main rectangular shape towards the north face and this portion has its own foundation at a higher soil elevation, but is connected to the structure by its grade beams that attach to the top of the basement shear walls.

Figure 3.5. Foundation During Retrofitting.

Figure 3.6. Aftermath of Conference Saloon Removal.

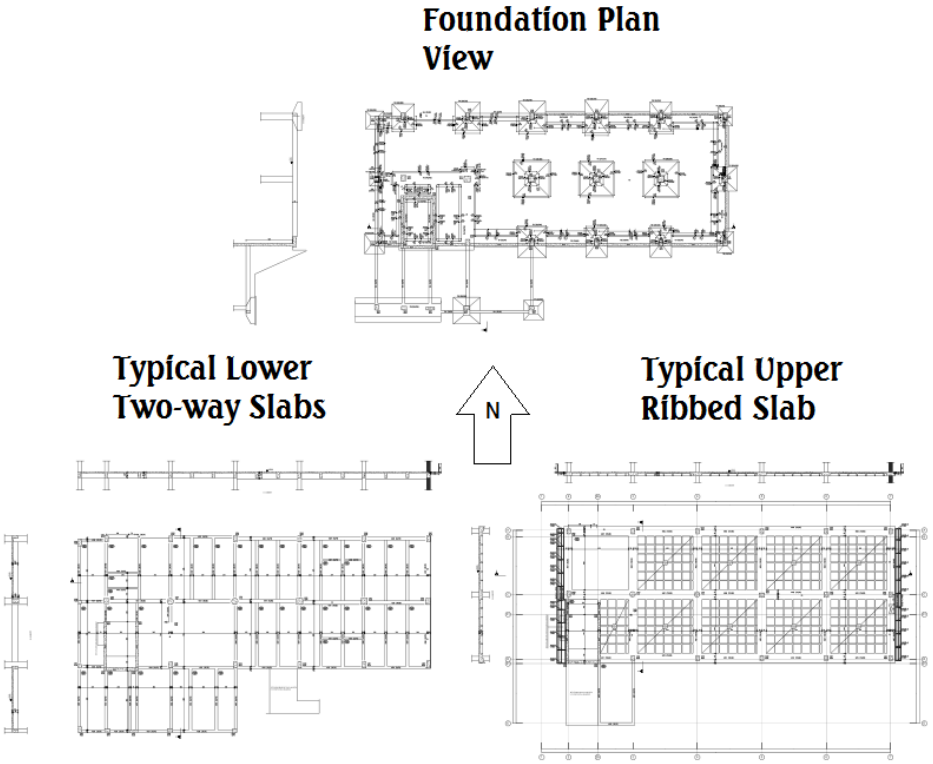

Figure 3.7. Floor and Foundation Plans.

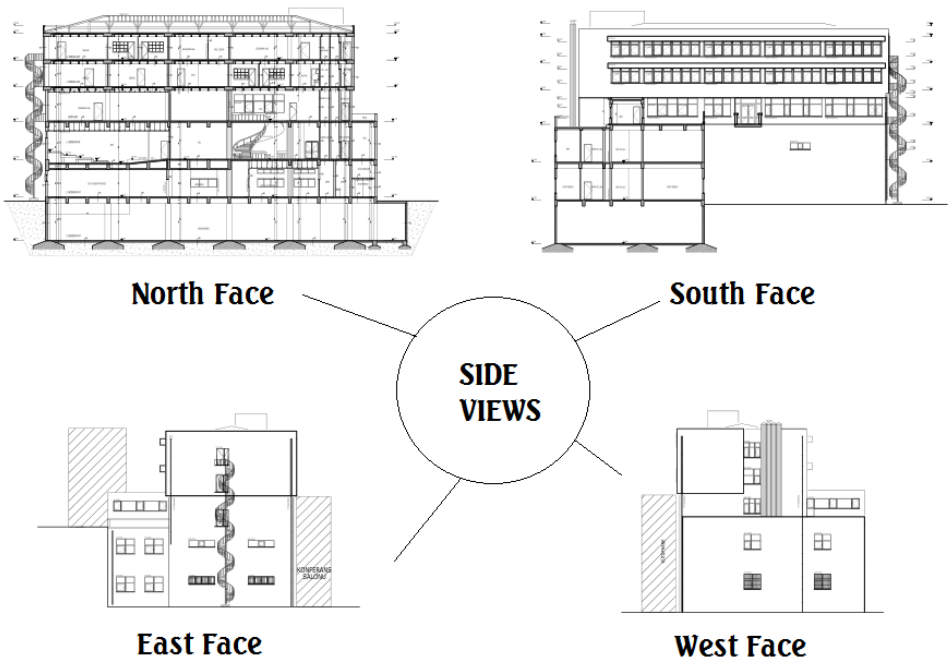

Figure 3.8. Side Views of ETA-B.

3.3.2. Ambient Vibration Analysis of ETA-B Building

ETA-B Building has been monitored simultaneously with eight triaxial force-balance type accelerometers in different instances of its retrofitting process. The first set of measurements (OMA) are taken before major demolishing activities, but the structure was emptied for the retrofitting process. The second set of measurements (OMA) are taken at a time when most of the infill walls were taken off and some of the columns were missing their concrete covers. Additionally, the excavation work around the footings and grade beams, down to the depth of soil contact surface of the foundation was complete. One basement structural wall and the surrounding soil was removed for easy access to the basement from east face of the building and although at a slow pace, there were ongoing demolishing work at the top 3 floors. The third set of measurements (FVA and OMA) are taken after the retrofitting was done and are not included in this study.

Table 3.1. Sensor Distribution Table.

Level No.	**First Set of Tests**	**Second Set of Tests**
Level -1	a, b	d
Level 0	a, c	d
Level 1	a, c	d
Level 2	a, c	d
Level 3	–	d
Level 4	–	d
Level 5	–	d, e

The sensor locations in a typical floor are given in Figure 3.9 and Table 3.1 shows the distribution of the sensors at each level in relation to the locations in Figure 3.9.

Although both OMA cases were analyzed, only the second set of tests are used for model updating, since these allow for determination of mode shapes throughout the full height of the structure. Figures 3.10a and 3.10b show the singular value lines for

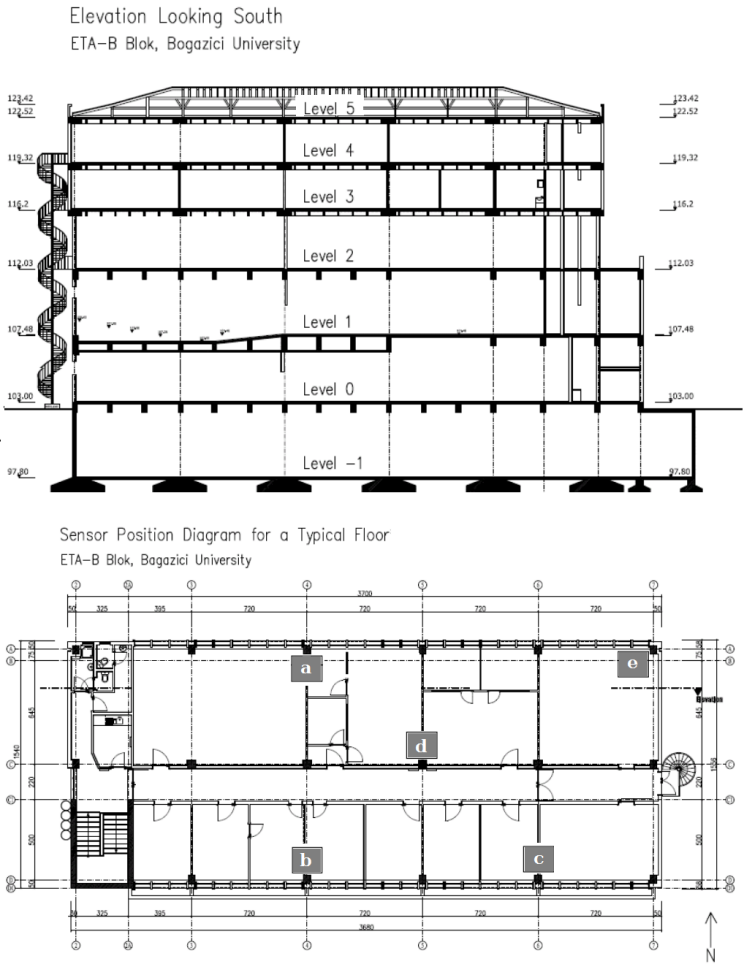

Figure 3.9. Sensor Positions Diagram.

the first and second set of OMA tests, respectively.

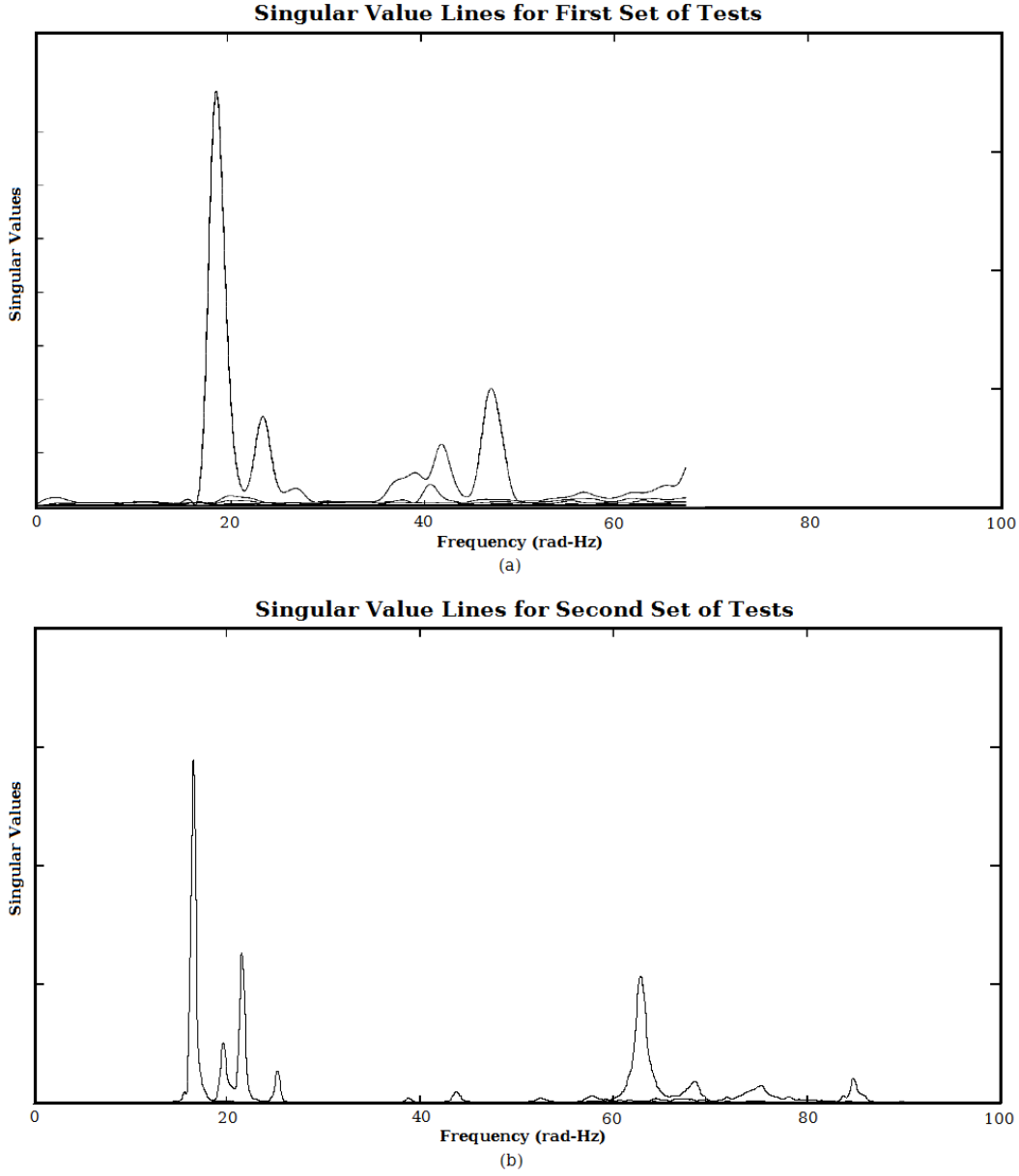

Figure 3.10. Singular Value Lines Obtained by EFDD Method.

Figure 3.11 shows the impulse response function of the first mode, obtained from first and second set of OMA tests. It is important to note that the removal of the masonry infill walls can be seen to greatly reduce the amount of damping, especially in the first mode of the structure. Table 3.2 and Table 3.3 give the modal parameters extracted from the first and second set of tests, respectively.

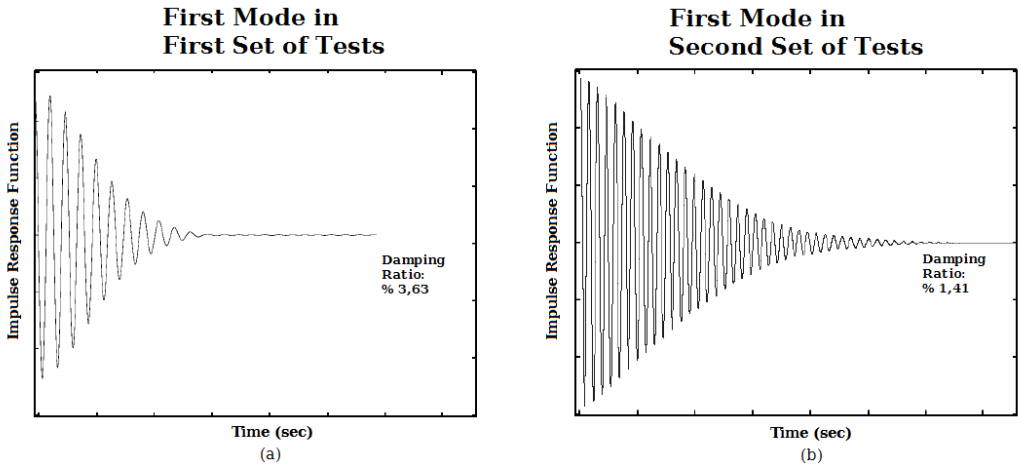

Figure 3.11. Impulse Response Functions Obtained For the First Modes.

Table 3.2. System Identification Results of ETA-B Building in First Set of Tests.

Mode No.	**Natural Frequency,** w_i	**Modal Damping Ratio,** ξ_i
1	18.51 (rad-Hz) $\equiv$ 2.94 (Hz)	0.04
2	23.30 (rad-Hz) $\equiv$ 3.71 (Hz)	0.03
3	26.51 (rad-Hz) $\equiv$ 4.22 (Hz)	0.03
4	41.76 (rad-Hz) $\equiv$ 6.65 (Hz)	0.02
5	46.89 (rad-Hz) $\equiv$ 7.46 (Hz)	0.02

Table 3.3. System Identification Results of ETA-B Building in Second Set of Tests.

Mode No.	**Natural Frequency,** w_i	**Modal Damping Ratio,** ξ_i
1	16.52 (rad-Hz) ≡ 2.63 (Hz)	0.01
2	19.60 (rad-Hz) ≡ 3.12 (Hz)	0.02
3	21.55 (rad-Hz) ≡ 3.43 (Hz)	0.01
4	25.19 (rad-Hz) ≡ 4.01 (Hz)	0.01
5	38.77 (rad-Hz) ≡ 6.17 (Hz)	0.01
6	43.67 (rad-Hz) ≡ 6.95 (Hz)	0.01
7	52.40 (rad-Hz) ≡ 8.34 (Hz)	0.01
8	57.74 (rad-Hz) ≡ 9.19 (Hz)	0.01
9	62.71 (rad-Hz) ≡ 9.98 (Hz)	0.01
10	68.36 (rad-Hz) ≡ 10.88 (Hz)	0.01
11	75.21 (rad-Hz) ≡ 11.97 (Hz)	0.02

The mode shapes can be seen in Figure 3.12 and Figure 3.13 for first and second set of OMA tests, respectively. In the first set of tests, the mode shapes are normalized against the rigid body motion of foundation along the vertical set of sensors in location "a" in Figure 3.9. Due to lack of a sensor in location "c" at the basement level (Level -1), the vertical set of sensors along location "c" can not be shift corrected, efforts to extrapolate from location "b" can not yield any results since, rigid body motion assumption for the basement level shift requires motion definition of a plane, which can only be defined by at least 3 points. Therefore, only sensors at location "a" are drawn for mode shapes from first set of tests.

For second set of tests, 7 sensors lie on a vertical line along location "d" in Figure 3.9 and only one sensor is at location "e", which is as described above not shift correctable in modeshapes. Therefore, it is also neglected in the mode shape drawings in Figure 3.13 and it is also not considered for model updating process.

For the second set of tests, the strongest two modes are a combination of twist

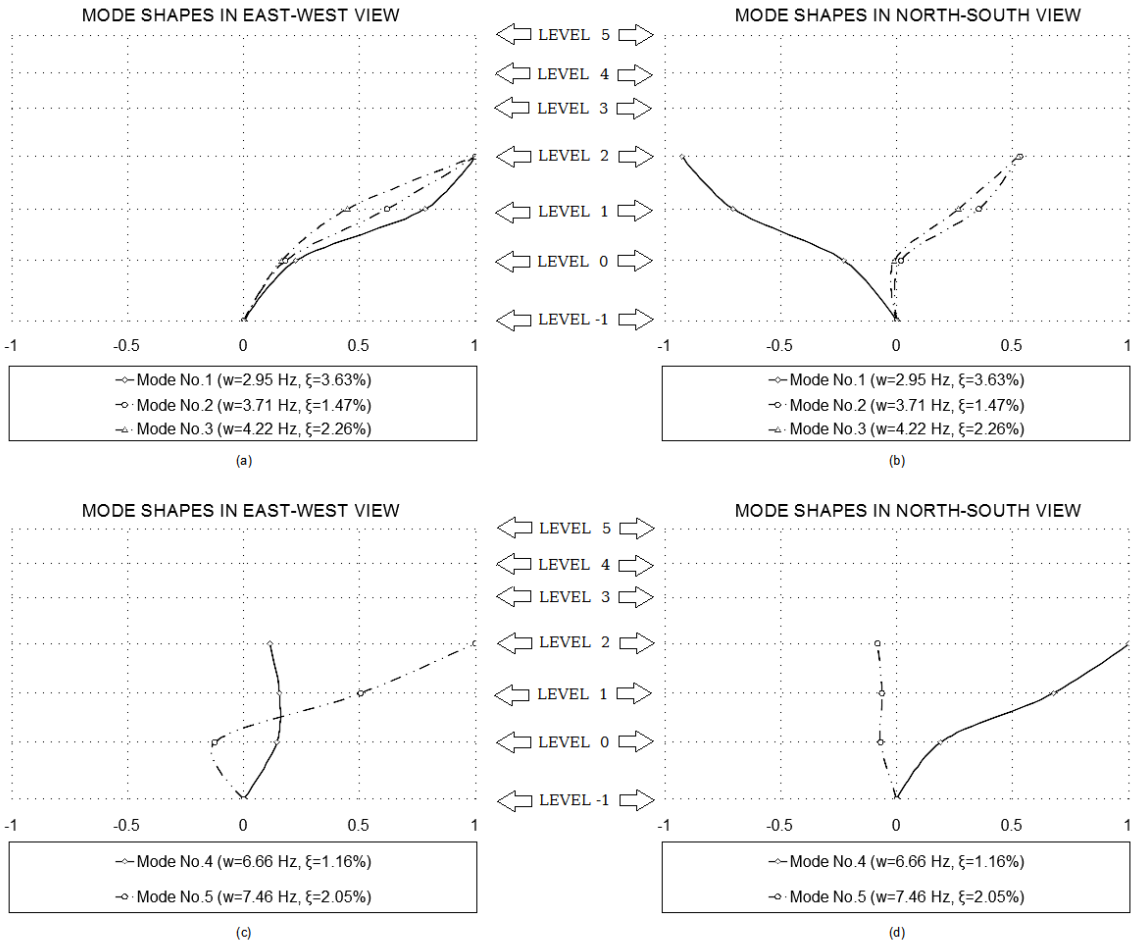

Figure 3.12. Mode Shapes of ETA-B Building in First Set of Tests.

and sway in X and Y directions. Almost all modes are complex, meaning that there are no pure X or Y sways. This is due to the rigidity imbalance caused by the corner location of shear walls around the stairs. A torsional mode that rotates around this shear wall is dominantly present in the first modes. It shall be noted that the 2nd, 3rd and 4th modes are almost the same in second set of tests. This has become a crucial factor in the model updating process.

One further note is to be given about the damping ratios found for the modes. Although, the first mode's impulse response functions as seen in Figure 3.11 seem rather unaffected, the following modes exhibit increasing amounts of distortion in IRF due to *beating* phenomenon. This adversely effects the damping estimate as discussed in [37]. The accurate extraction of damping ratio is not achieved to the full extent in the development of the current code used for this thesis even without the presence of *beating*. The accuracies in [27] was not obtained. Damping ratio's extracted are generally on the order of $\pm 75\%$ proximity to the actual values in the test runs made with synthetic data. (i.e. a result of $\xi = 0.03$ would approximately mean $0.01 \leq \xi \leq 0.05$) Therefore, the error due to *beating* is not confronted for damping estimates.

However, the validation tests made for the code written have yielded almost exact results for natural frequencies and mode shapes, which are to be used for model updating purposes.

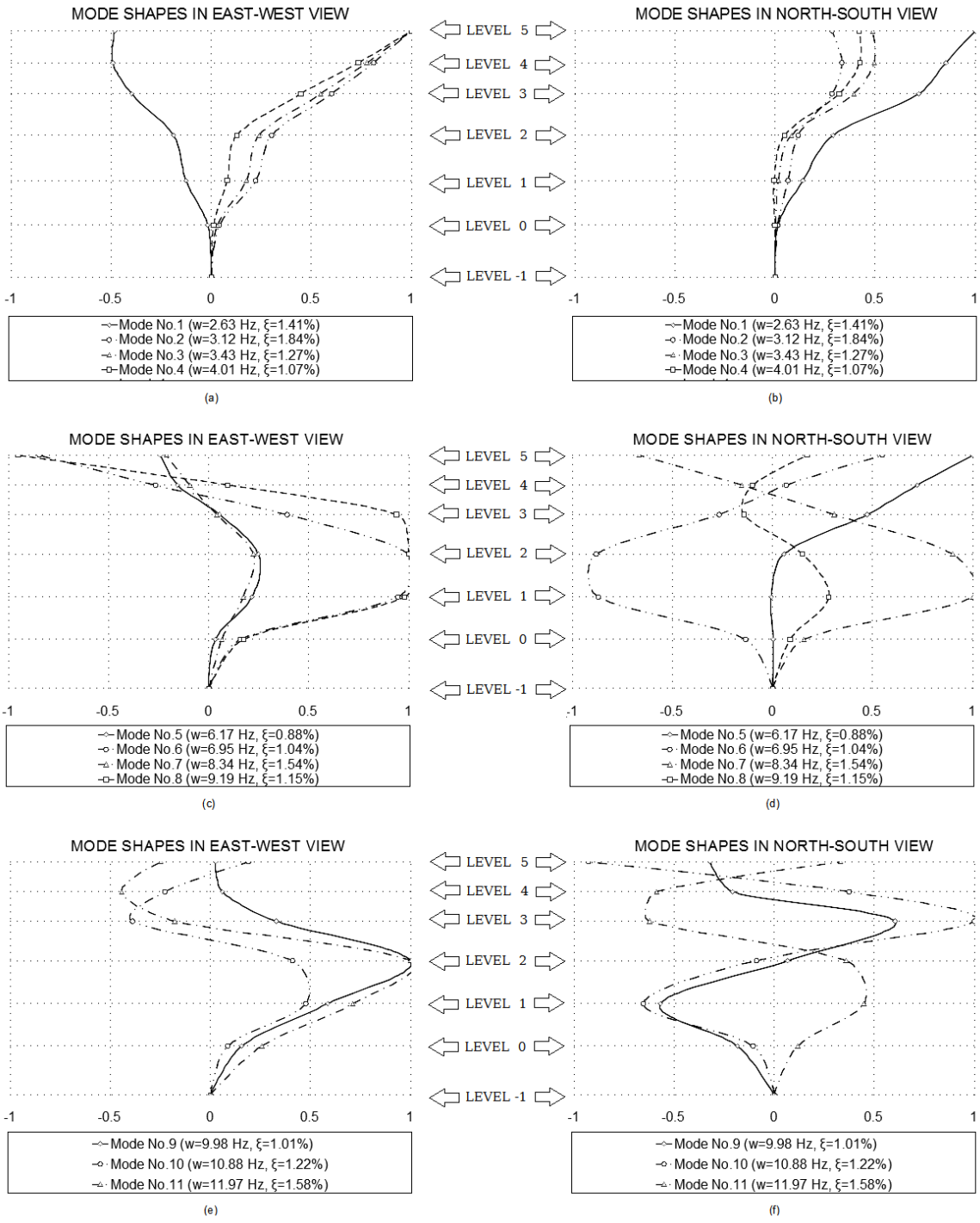

Figure 3.13. Mode Shapes of ETA-B Building in Second Set of Tests.

4. FEM OF ETA-B BUILDING

4.1. Modelling Overview

The FEM development for SHM is distinguished from model development for design purposes, since the desire is to update the model prior to any analysis. Particularly when modal parameters are extracted from ambient vibration testing, these models shall resemble the structure under operational conditions. This is the complete opposite of the design case, where the model is developed for the conservative simulation of earthquakes.

The modal parameters to be used in model updating shall be carefully screened against false modes to which the FEM shouldn't be able to converge. A fundamental issue is on the dynamic interaction between closely spaced buildings. The effect of rotating machinery can be seen in singular value lines in FDD technique, i.e. as needle like sharp peaks and they can be identified as nonstructural easily (This may prove difficult if, it is close to a structural mode, and even may bias the mode shapes found.).

One such example can be found on a plumbing engine in the basement of a monitored structure in [38]. But more importantly, in [38] the effect of dynamic interaction of close by buildings are discussed. The identification of dynamic interaction due to close by structures is harder since they do not manifest themselves as apparently as in rotating machinery. In [38] the issue is resolved by simultaneously monitoring close by structures as well and having many identification algorithms work together to justify or discriminate a mode.

Although less stressed, the effect of dynamic interaction between close by buildings is also realized in [39], where the obtained modal parameters change with demolishing of close by buildings. The issue of non-structural component's effect on the modal parameters identified is also seen here through removal of these prior to the structure's demolishing.

Another area of interest for setting up the initial FEM to be updated along with OMA modal results is the question of modelling of soil-structure interaction. It is seen in application that in [40], fixed base assumption for the foundation, and in [39], disregard of soil structure interaction for the first modes for soils with good characteristics is considered agreeable. Yet, the immense variability in possible soil conditions at the site and its way of interaction is a big unknown. There are additional questions to be asked concerning the possible effects of ground water levels in the soil structure interaction.

One final note is on nonstructural elements' and masonry infill walls' effect in OMA testing. Especially for masonry infill walls, the approach to modelling for FEM updating and also for seismic evaluation shows a scatter between studies. Assuming a closely representative FEM is somehow achieved, seismic evaluations can be based on *nonlinear* (compression) only equivalent struts in nonlinear time history analysis for performance based assessments. This alone poses assessment problems due to fact that the likely failure type of the walls are unknown. They can range between 25 different types according to [41] and they can cause plastic hinges not anticipated to develop in an earthquake scenario [41]. This situation is closely effecting the reliability of SHM made. Information on how masonry walls behave under operational conditions rather than failure conditions could improve the OMA related updating of the FEM.

In updating, modal parameters can be found only in a linear analysis, which can not incorporate compression only members, which are considered nonlinear. Generally, modelling of the masonry walls is done in equivalent struts in most of the studies, without regard to tension actions of the defined struts.

It shall be noted here that "linear iterative modal analysis" described in [42], tries to overcome this issue, by iteratively deleting struts that are found to be in tension in the modal analysis, until there are no tensioned struts for a given mode shape. But, a natural question arises for the uniqueness of such a solution with regard to which struts are left in a mode.

The inability to correctly account for the effect of nonstructural elements, especially compression only elements such as masonry walls, or otherwise inherently nonlinear behavior, as they actually behave under operational conditions, could lead to physically unrelated, but nonetheless updated FEMs, which would pose a significant reliability issue for the SHM made.

4.2. Model Development

The Finite Element (FE) model development for ETA-B building has taken numerous attempts and a long trial and error period. The reasons for this are both the lack of a complete set of original structural drawings and out of the ordinary geometric features of ETA-B, such as slab systems designed essentially for obtaining a valley shape inside a classroom for enablement of best viewing angles from back rows of the class.

At the time of the testing, utility items, such as desks, tables and furniture, are known to be transported out of the structure, so the structure is more or less empty. Despite this, the mass of the structure is tricky to model. The geometry is comprised of ribbed floors at the upper 3 storeys, which cause, when calculated with disregard of the overlap of the members at the nodes, calculation of extra masses that heavily influence the modes of the structure. Especially due to its location being the top floors. Unaccustomed construction practices and forgotten ones influence the mass further. One such example is addition of a layer of a centimeter of cement mortar to the roof slab each year for water isolation. This alone causes 33 cm of cement layer mass for entire floor area (Testing was done in 2010 and the building is estimated to be dated c. 1977.). Additionally, in the second set of OMA tests, which are carried out after some de-construction activity has taken place, the uncertainty on mass of nonstructural elements increase due to unknowns such as number and location of remaining masonry walls and distribution of pallets used for storage of new tiles, sinks and windows throughout the structure.

At several locations, the architectural drawings available are misleading, it is

possible that structure is either altered in its 33 years of usage or decisions were made that are separate from the original plans as the building progressed in construction. Some of these changes might have been obligatory, one example to this is the foreseen car park beneath the ETA-B building in original plans. From Figure 3.5, we can see that the ground water table is in conflict with such an expansion underneath the structure. This also raises questions, as to whether or not any soil investigation was done in the first place.

After numerous trials and errors the connection in Figure 4.1 for reinforced concrete members were deemed adequate, along with frame insertion points to realize the actual locations of the cross-sections of these frames in a connection.

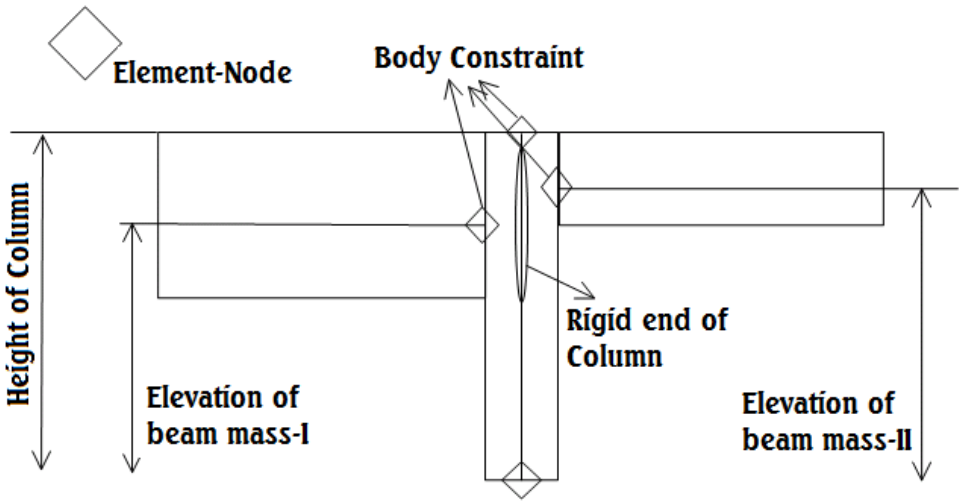

Figure 4.1. Frame Connection Details.

CSI's SAP2000, [43] FEM software has been used in the development of the model. Each frame object is characterized by two nodes and a center line between them. Frame insertion point property in SAP2000 allows for the modification of the stiffness of the member as if it lies on a different lengthwise line other than direct connection between the nodes. This is useful for making the actual geometric alignments effect the joint stiffnesses. Frame insertion points change the stiffness of the elements accordingly but the mass of the object is still lumped at the nodal positions, this condition may cause the full mass of a story to be modeled at an elevation or lateral shift. Therefore, where

considered necessary the definition of the nodes are altered instead of using only frame insertion points. But, the alignment of the columns are stiffness wise adjusted via frame insertion points, since these contribute relatively less to the total mass of the structure. The error due to misalignment of column masses by a few centimeters is neglected.

Figure 4.1 shows the nodes of these elements as not directly connected to each other, this is done to avoid mass overlap at the joints, which cause large amounts of unwarranted mass to be incorporated into the model especially at the ribbed slabs of the upper floors. The connection between the nodes of the elements at a joint is however made possible via *body constraints*, which can include translational or rotational degrees of freedom to be fixed. The relatively extra stiffness of the joints at locations where beams and columns interlock are modeled as rigid end offsets for the columns along the shared length of the columns with the depth of the beams. This condition is necessary to simulate the behavior under ambient vibration conditions, since the relative motion at these locations are fairly limited due to rebars continuing into connecting elements and tie spacing reductions.

The above described modelling approach is highly labor intensive for large structures or structures at sizes comperable to ETA-B, therefore, it is advised for any new researcher to use SAP2000 API for automating the structural definitions or use a fully programmable FEM software such as OpenSees. The developed FEM for model updating with second set of OMA tests, in which some de-construction has taken place, can be seen in Figure 4.2.

The foundation is modeled as fixed connections at the footing locations and the elevation shifted north-side foundation that connects to the top of the basement shear walls via grade beams is modeled as a separate set of fixed supports at its footing locations. A trial and error procedure was then undertaken for modelling the interaction between the grade beams at this foundation and the top of the basement shear walls they connect to. However, the approaches tried have turned out to greatly reduce the MAC values of the matching modes in OMA extracted mode shapes, therefore this

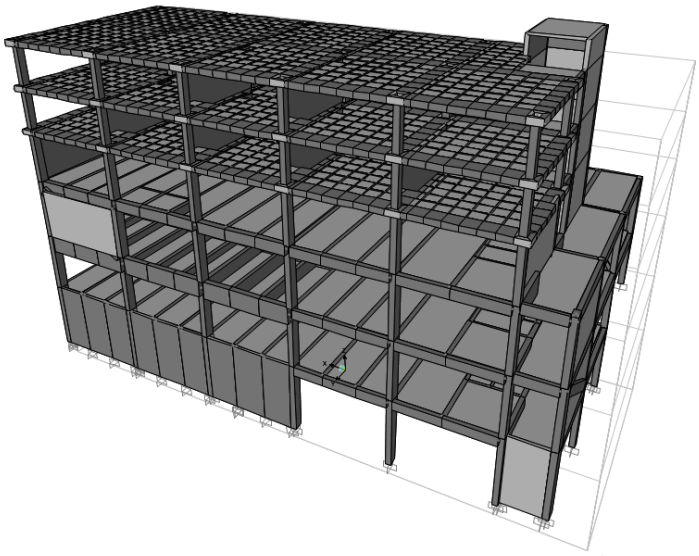

Figure 4.2. ETA-B Building FEM.

effect is eventually neglected.

The soil-structure interaction is neglected in this model, since the pictures from the retrofitting process suggest soil that is capable of withstanding gravity loads at sharp slope angles is surrounding the basement shear walls, and the soil-structure interaction for strong soils under OMA testing could be ignored [39].

Slabs inside the beam enclosements are modeled with nodes placed in such a way to avoid extra mass calculation due to slab-beam overlaps. And, their connections are made possible via body constraints with full fixity at the nodes. The configuration is independently checked for independent motion of beams and slabs at the perimeters of the area elements defined, which shall be avoided. All area elements, including shear walls and slabs are modeled as *thin-walled shell* area elements to make shear deformations on these elements to be accounted for (CSI SAP2000 reference manual can be used to compare other area elements such as thick-walled or plate elements.).

The 1975 Seismic code, [22] has been utilized to calculate parameter ranges for

columns, beams and shear walls in a simplistic manner. From the ranges of possible concrete classes envisioned in design and associated steel reinforcement ratios mentioned in the 1975 code, equivalent homogeneous young's modulus ranges are calculated and the non-updated model is parametrized with an intermediate value for the members.

Table 4.1. Relevant 1975 Seismic Code Provisions for Parameter Range Calculations.

Section	**Provision**
6.6.3	Longtidunal steel reinforcement in columns is at least 1% and at most 3% for B160 3.5% for B225 4% for B300 (where concrete classification is made via B-compressive strength) Use of higher strength steel than BÇ-II (S420) is not allowed
6.7.2	Minimum reinforcement ratio for structural walls can not be less than 0.25% for lateral and 0.2% for longtidunal reinforcement. Spacings can not be greater than 1.5× wall thickness and 30 cm
6.9.2	Beams can not have reinforment ratios below 0.5% for BÇ-I steel 0.4% for BÇ-II steel (S420) 0.3% for BÇ-III steel (Same ratios apply to slabs)

The code envisions 3 classes of concrete in the minimum and maximum steel reinforcement constraints, the tangential modulii of these can be calculated from the Hognestad curve as,

- B160 $E = 20,040$ MPa
- B225 $E = 23,030$ MPa
- B300 $E = 26,480$ MPa

We can assume that at the strains the building is operating under, the ties can

not deform and thus can not introduce strength increase in the concrete, therefore, the tangential values can be used for the concrete in the following equivalent material (Young's) modulii calculation.

Table 4.2. Parameter Range for Column Equivalent Material Modulii.

Concrete	Steel Ratio	Young's Modulus
B160	1%	22,040 MPa
B160	3%	26,040 MPa
B225	1%	25,030 MPa
B225	3.5%	30,030 MPa
B300	1%	28,480 MPa
B225	4%	34,480 MPa

Therefore, the column stiffnesses may lie anywhere between 22 to 35 GPa without consideration for creep, shrinkage or corrosion and assuming perfect match of design with construction.

Assuming minimum reinforcement for shearwalls, we can obtain,

Table 4.3. Parameter Range for Shearwall Equivalent Material Modulii.

Concrete	Steel Ratio	Young's Modulus
B160	0.2%	20,440 MPa
B225	0.2%	23,430 MPa
B300	0.2%	26,880 MPa

Therefore, the structural wall stiffnesses may lie between 20 to 27 GPa, without consideration for aging and with minimal reinforcement.

Assuming BÇ-II (S420) steel being used (giving the middle case for 3 alternatives in minimum steel ratios), the minimum steel ratio is 0.4% for beams and slabs. With

Table 4.4. Parameter Range for Beam and Slab Equivalent Material Modulii.

Concrete	Steel Ratio	Young's Modulus
B160	0.4%	20,840 MPa
B225	0.4%	23,830 MPa
B300	0.4%	27,280 MPa

this additional assumption to the preceding cases, the stiffness of the beams and slabs can be approximated to lie between 20 to 28 GPa.

As for mass calculations the following base weight units are utilized. The values are given in weight (not mass) to keep ease of comparison of the values to the accustomed design loads in civil engineering. (with $9.81 m/s^2$ gravitational acceleration)

Table 4.5. Basis for Mass Calculations.

Material	Weight
Cement Slurry	$14.15 kN/m^3$
Cement Mortar	$21.21 kN/m^3$
Reinforced Concrete	$24 kN/m^3$
8.5 X 19cm Clay brick	$0.021 kN$
Clay Roof Tile	$0.40 kN/m^2$
Pine Tree	$5.2 kN/m^3$

Following the above base units, the mass of two common types of masonry walls, one with 19 cm thickness and one with 8.5 cm thickness, have been calculated with consideration of wall finishes (1-2cm on one face typically) and current industry standards for coverage of a m^2 (25 $pieces/m^2$ or 50 $pieces/m^2$ depending on which brick side is utilized). This way, $11.76 kN/m^3$ for 19 cm thick walls and $7.89 kN/m^3$ for 8.5 cm thick walls have been obtained.

The masonry walls are initially modeled as equivalent compression struts following the Sucuoğlu and Mc.Niven 1991 formulation [44], without mass, and the mass of the masonry walls were included in the model as area objects with mass and zero stiffness. The effect of openings in masonry walls was ignored, since the clear effect of the masonry walls on mode shapes and frequencies was thought to be unattainable with the approach tried in [45], after findings of fairly low strength wall stiffnesses.

However, model updating trials without linear iterative modal analysis (as in [42] to assure each strut in action is in compression) have yielded unrealistic convergence values for the masonry walls, therefore this approach is eventually changed to incorporate area elements as stiffness providers in masonry wall modelling (with 0.17 poisson ratio).

Masses of wooden roof truss (assumed to be pine), roof tiles and the 33 cm cumulative water isolation cement have been calculated to a sum of 334 kN and is distributed equally to the already dense nodal mesh of top story slab (due to modelling of ribbed slabs, there exist $3,043$ joints in this one floor only)

4.3. Model Updating of ETA-B Building

Iterative model improvements (as in [1]) have allowed the model to mature enough for a parameter study. Young's moduluses of structural walls, columns, beams, slabs, masonry walls and specific weight of concrete members are selected as update parameters. A parameter study for varying values of update parameters has been done with regard to first 4 modes of the structure.

It is evident from the mode shapes extracted from OMA that the 2nd, 3rd and 4th modes are essentially the same in shape as can be seen in Figure 4.3.

This may be caused by the constraints on ETA-B building that are not modeled. These include North-South direction contact with the conference hall for up to two and a half storeys and the similar contact of rectangular extension section of the ETA-B

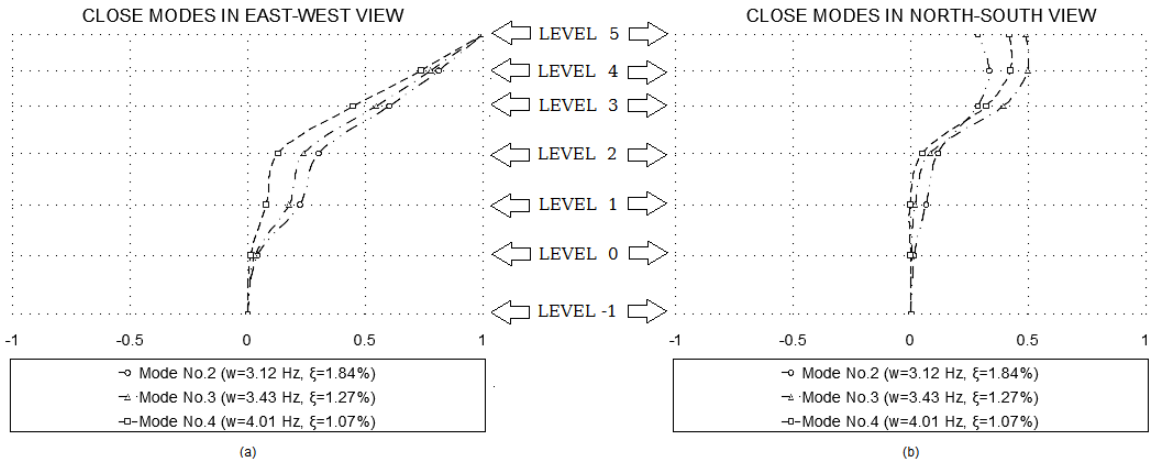

Figure 4.3. Close Modes of ETA-B.

with another building to the south. It is important to realize that the mode shapes mentioned also diverge in east-west direction and converge in north-south direction from approximately the height of the conference hall contact.

The effect of such a contact can not be modeled linearly, since the contact structure resists motion towards it, but does not pull back the structure like a spring. The situation is very similar to that of a soil pressure distribution under a footing, which can not apply tension.

Since, this effect can not be modeled linearly as a spring, the 2nd, 3rd and 4th modes are found to converge on the 2nd mode of the FEM with the frequency of the 2nd extracted mode and the shape of the 3rd extracted mode.

Therefore, the first two modes of the FEM are updated with the first 4 modes extracted from OMA as described above. The MAC matrix of the nonupdated FEM can be found in Figure 4.4 and Figure 4.5, also the nonupdated model's parameter values are given in Table 4.6.

From this nonupdated model, the selected parameters are varied for a range of values and the results are plotted for decision making. It is assumed that since

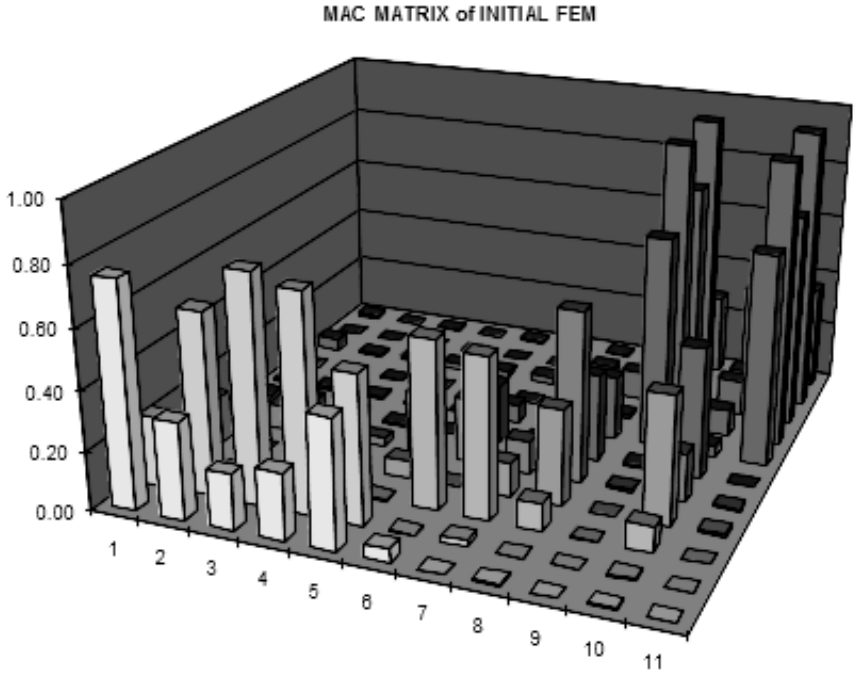

Figure 4.4. Non-updated FEM's MAC Matrix in 3D.

F	1	**0.76**	0.23	0.07	0.16	0.03	0.03	0.01	0.00	0.04	0.00	0.01
E	2	0.33	**0.62**	0.00	0.00	0.08	0.04	0.01	0.00	0.01	0.00	0.00
M	3	0.19	**0.77**	0.00	0.00	0.08	0.02	0.01	0.00	0.01	0.00	0.00
	4	0.23	**0.73**	0.00	0.01	0.03	0.01	0.00	0.00	0.02	0.00	0.00
M	5	0.43	0.50	0.01	0.06	0.21	0.00	0.00	0.00	0.02	0.00	0.01
O	6	0.05	0.01	**0.57**	0.00	0.22	0.21	0.06	0.00	0.03	0.00	0.05
D	7	0.00	0.02	**0.54**	0.11	0.11	0.04	0.00	0.01	0.00	0.03	0.01
E	8	0.01	0.00	0.09	0.32	**0.58**	0.30	0.22	0.01	0.10	0.00	0.00
S	9	0.00	0.00	0.00	0.00	0.01	0.01	**0.72**	**0.98**	**0.79**	**0.97**	0.28
	10	0.01	0.01	0.09	0.43	0.16	0.44	0.03	0.09	0.12	0.09	0.32
	11	0.00	0.00	0.00	0.01	0.01	0.00	**0.72**	**0.97**	**0.73**	**0.97**	0.36
		1	2	3	4	5	6	7	8	9	10	11
		O	M	A		M	O	D	E	S		

Figure 4.5. Non-updated FEM's MAC Matrix in 2D.

Table 4.6. Nonupdated Model Parameter Values.

Parameter	**Value**	**Units**
Young's Modulus of Structural Walls	24	GPa
Young's Modulus of Columns	30	GPa
Young's Modulus of Beams	24	GPa
Young's Modulus of Slabs	24	GPa
Young's Modulus of Masonry Walls	1.5	GPa
Specific Weight of Concrete	24	kN/m^3

the model updating problem is linear, similar gradients of MAC values and errors in frequencies shall be achieved at points other than the nonupdated parameters in the variable space. These graphs can be found in Figure 4.6 and Figure 4.7.

From Figure 4.6 and Figure 4.7, it can be seen that the parameters can be ordered in sensitivity as;

- Young's Modulii of Masonry Walls
- Young's Modulii of Beams
- Young's Modulii of Structural Walls
- Young's Modulii of Columns
- Young's Modulii of Slabs
- Specific Weight of Concrete

Specific weight of concrete and Young's modulii of Slabs are the most irresponsive items in the above list, with little to no effect on the MAC values. As for Young's modulii of columns and structural walls, MAC values and frequency values improve almost linearly with increasing stiffness, but the gradient is too small and the values continue to show linear improvements almost without bound (including unrealistic values as 100 GPa modulii for columns). This has led to their limitation based on the maximum value computed for concrete members in the model development section,

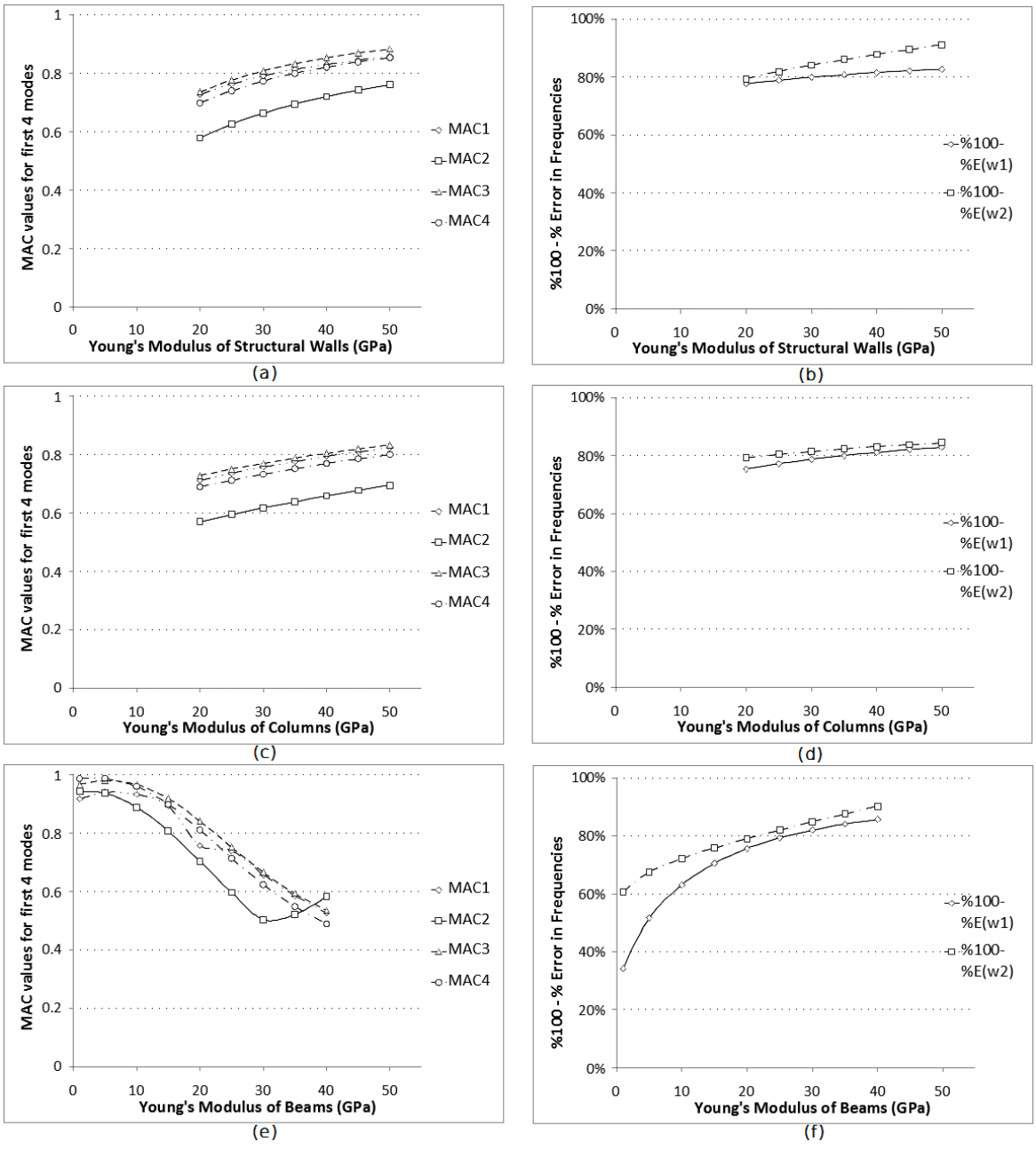

Figure 4.6. Change in Modal Values Through Change in Parameters - I.

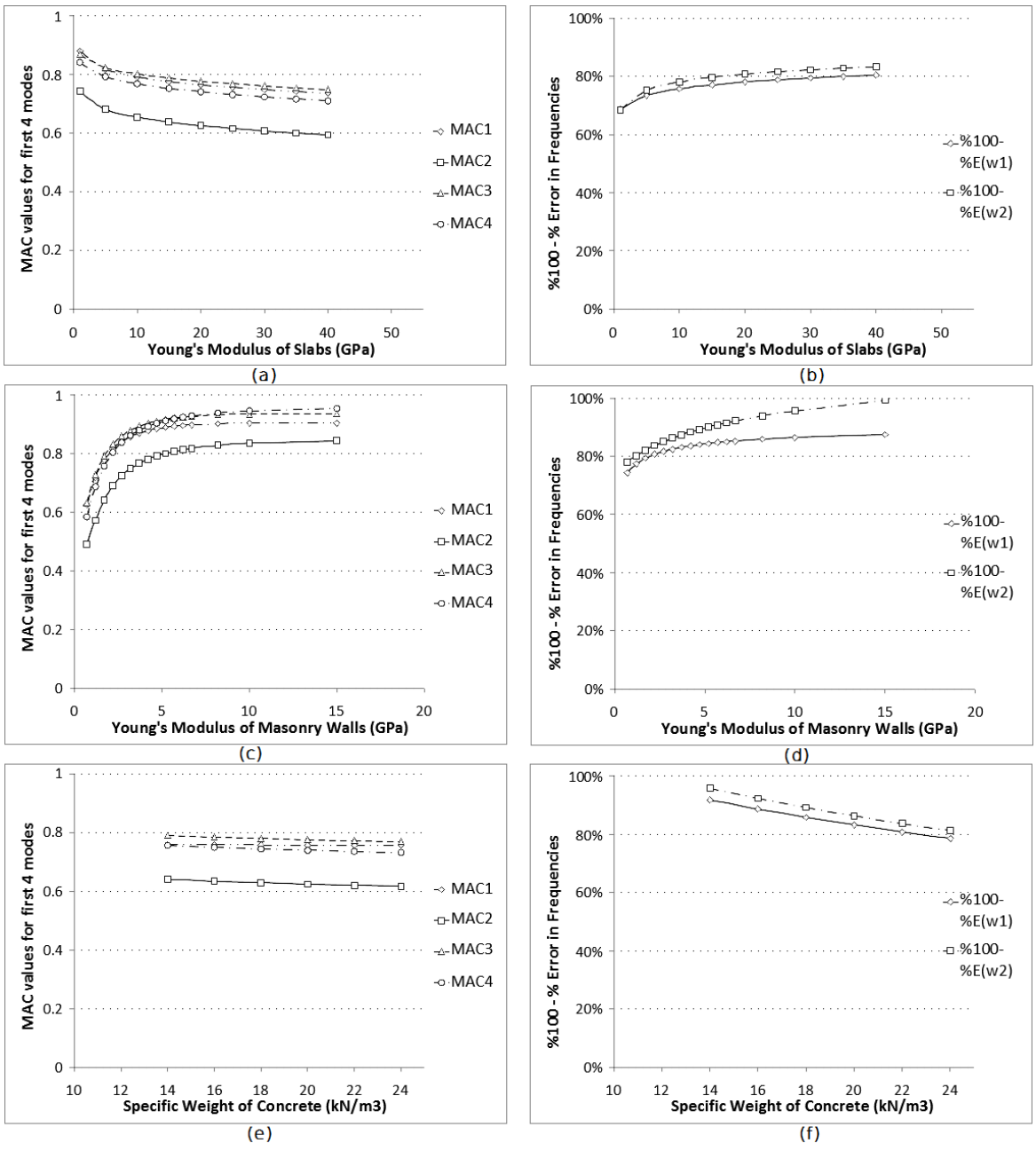

Figure 4.7. Change in Modal Values Through Change in Parameters - II.

which is 35 GPa.

The most sensitive parameters are the modulii of masonry walls (defined as area elements) and beams. Masonry walls show a fast convergence in Figure 4.7, such that after 6.7 GPa value is reached the additional contribution of succeeding modulii increments in MAC values and frequencies almost reduces to zero. It shall be noted that the values inferrable from the literature generally vary between 700 MPa to 3.7 GPa. The converged value of 6.7 GPa is in that sense quite high, but this could have been a result of some particular construction practices. As a potential candidate, practice of constructing the masonry walls before the columns to reduce the usage of formwork may increase the bondage and interaction between the columns and the walls to yield high stiffness values for the masonry walls as a whole.

Table 4.7. Updated Model Parameter Values.

Parameter	**Value**	**Units**
Young's Modulus of Structural Walls	35	GPa
Young's Modulus of Columns	35	GPa
Young's Modulus of Beams	28	GPa
Young's Modulus of Slabs	26	GPa
Young's Modulus of Masonry Walls	6.7	GPa
Specific Weight of Concrete	24	kN/m^3

As for modulii of beams, the effect of modulii increase has conflicting effects on the MAC values and the frequencies. It shall be noted from Figure 4.6 that the effect on frequency correction is very strong, this disables the ability to reduce the beam modulii beyond a certain point, since the effect on MAC values is the second most effective after the masonry walls.

The updating can be achieved by first implementing the obvious parameter values such as 6.7 GPa for masonry wall modulii, and then fine tuning for the remaining parameters. After, some manual manipulation of the parameters, in the light of the

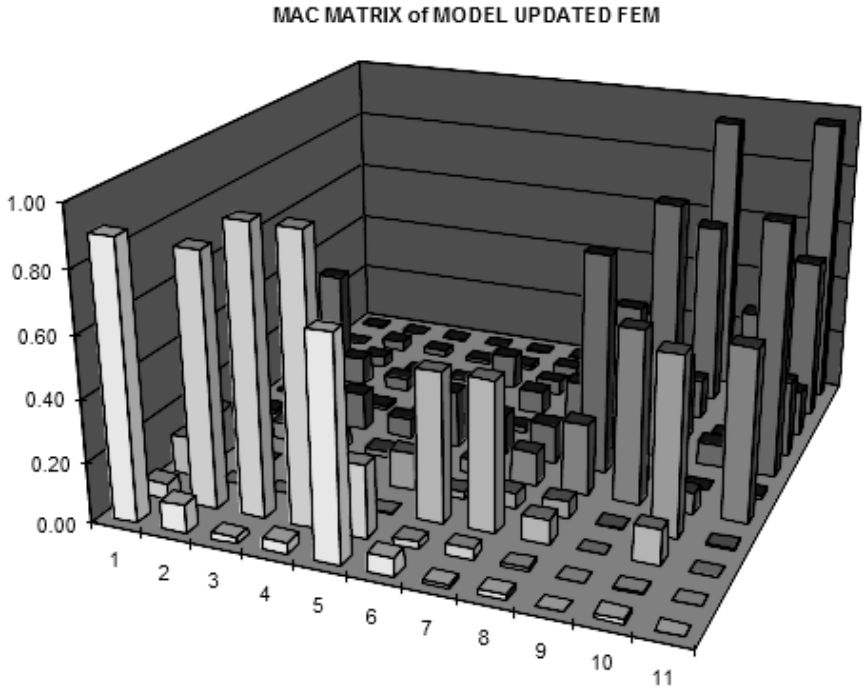

Figure 4.8. Updated FEM's MAC Matrix in 3D.

F	1	**0.90**	0.05	0.13	0.15	0.00	0.01	0.01	0.07	0.32	0.00	0.00
E	2	0.09	**0.83**	0.00	0.00	0.06	0.15	0.02	0.09	0.04	0.03	0.00
M	3	0.02	**0.93**	0.00	0.02	0.04	0.13	0.01	0.05	0.00	0.02	0.00
	4	0.04	**0.93**	0.00	0.01	0.02	0.07	0.01	0.03	0.00	0.01	0.00
M	5	**0.71**	0.24	0.00	0.12	0.05	0.19	0.00	0.00	0.12	0.02	0.00
O	6	0.06	0.02	0.49	0.02	0.05	0.14	0.02	0.08	0.05	0.04	0.00
D	7	0.01	0.03	0.49	0.05	0.11	0.13	0.00	0.13	0.04	0.07	0.03
E	8	0.02	0.01	0.08	0.06	0.23	**0.72**	0.13	0.43	0.55	0.08	0.00
S	9	0.00	0.00	0.00	0.00	**0.57**	0.01	**0.85**	0.27	0.14	**0.62**	**0.93**
	10	0.02	0.00	0.11	**0.58**	0.07	0.00	0.08	0.03	0.01	0.33	0.02
	11	0.00	0.00	0.00	0.00	**0.56**	0.01	**0.84**	0.25	0.15	**0.54**	**0.96**
		1	2	3	4	5	6	7	8	9	10	11
		O	M	A		M	O	D	E	S		

Figure 4.9. Updated FEM's MAC Matrix in 2D.

parameter studies, the values for the updated model are reached as in Table 4.7. The resulting MAC matrix can be found in Figure 4.8 and Figure 4.9.

As can be seen from the figures the MAC values are satisfactory (around 0.9) with the understanding that the 2nd, 3rd and 4th modes are converging to the second mode of the FEM as described previously. As for frequencies, the first mode is corrected from a 21% error to an 8% error (FEM:2.07 Hz vs. OMA:2.63 Hz) and the second mode is corrected from a 19% error to a 1% error (FEM:3.16 Hz vs. OMA:3.12 Hz). The updated FEM modes in dominant directions can be viewed in Figure 4.10.

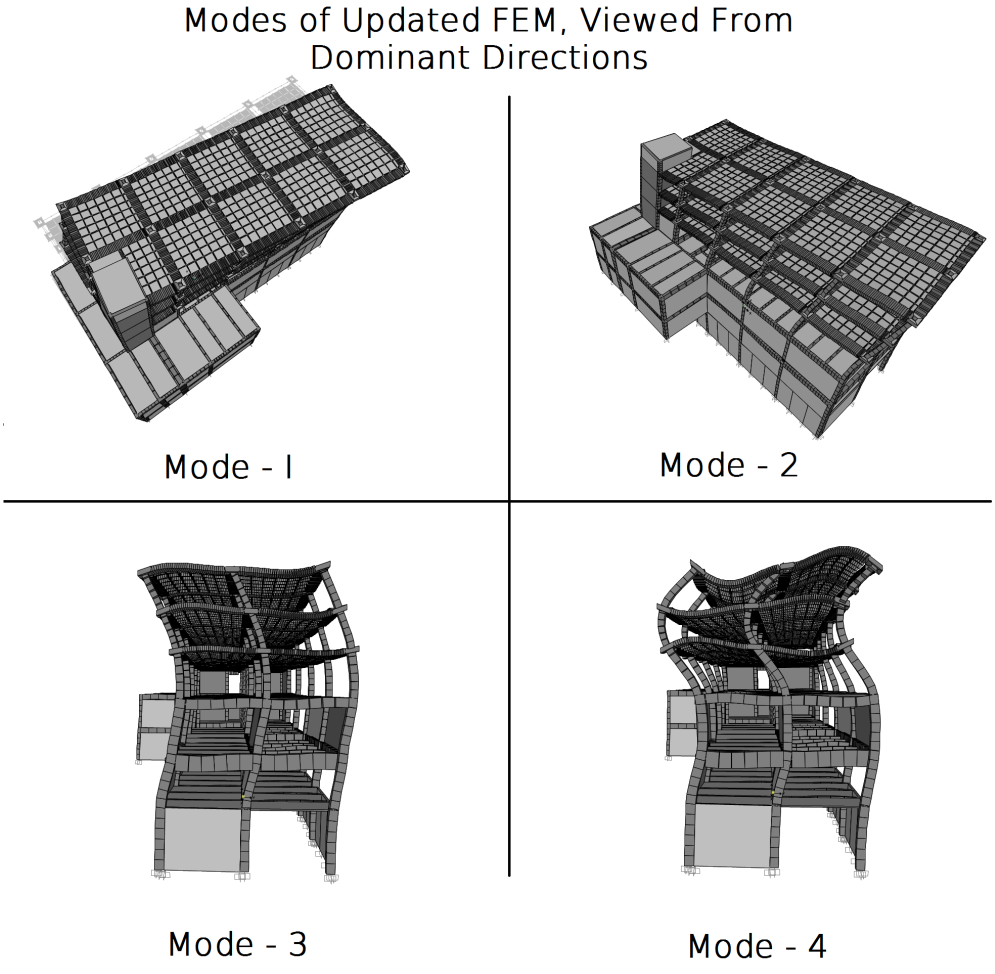

Figure 4.10. Updated FEM's First Four Mode Shapes.

4.4. Justification of Model Updating Results

In Section 4.2 the equivalent Young's moduluses of concrete members are calculated very simplistically, as if they are compression-tension only members. This facilitated for a starting point for the model updating to be made. The non-updated model gives frequency values lower than that of OMA results, therefore it is naturally expected that the modulii of the concrete members during the model updating process shall increase. However, since the initial modulii was calculated simplistically, a backwards check concerning the maximum allowable value of Young's moduluses of concrete members is required.

This is done via, picking a concrete column section and fictitiously reinforcing it to maximum allowed limits in the 1975 earthquake code. The section chosen is the most dominantly used column section (400 X 700 mm) at Level 0, the storey to yield the largest drift ratios according to results from Chapter 5.

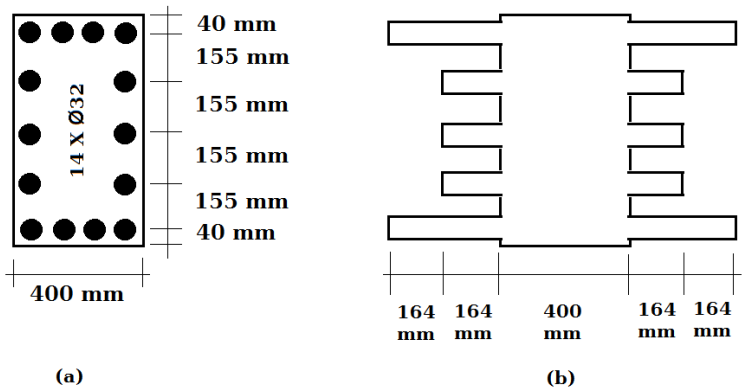

Figure 4.11. Fictitiously Reinforced Section and Its Uniform Material Transformation.

The section shown in Figure 4.11 is assumed to made of B300 concrete and reinforced to 4% reinforcement, which is the maximum allowed by 1975 earthquake code. To facilitate calculations, a fictitious reinforcement layout is assumed as in Figure 4.11a. If the steel areas are transformed into equivalent concrete areas, and the parallel axis theorem is utilized, a linear elastic (EI) rotational stiffness value can be calculated. Since, the area moment of inertias' are not altered in the FEM, an

equivalent Young's modulii can be calculated by dividing this value to the original area moment of inertia. This procedure results in the computation of 37 GPa and 36.5 GPa, for strong and weak directions, respectively.

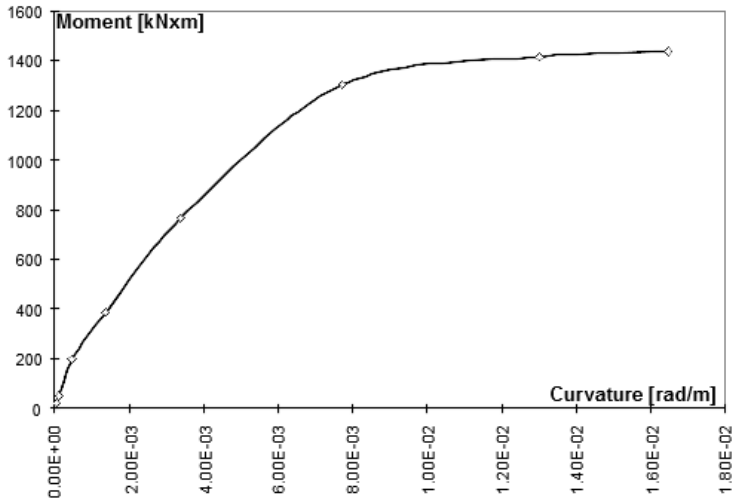

Figure 4.12. Moment-Curvature Diagram of Fictitious Column Section.

The maximum allowed Young's modulus to be reached by the model updating for a reinforced concrete member is calculated alternatively from the same section by plotting its moment-curvature relationship, Figure 4.12. The figure suggests a yield moment of 1,300 kNxm, (under 723 kN of compression load calculated for the column) around which the equivalent Young's modulus is 15 GPa. However, for very low curvatures (around or below $4.68 \times 10^{-}4$ rad/m) it is calculated to be around 36.8 GPa. These very low curvatures can be assumed for the conditions in which OMA testing is applied. (The effects of confinement are disregarded, however, at the strains considered for OMA the lateral reinforcements are not expected to contribute to a strength increase of the concrete)

Therefore, the maximum value reached during model updating, 35 GPa by the columns and the structural walls are agreeable.

5. STRUCTURAL ASSESSMENT OF ETA-B BUILDING

5.1. Performance Based Seismic Evaluation, an Overview

The expected damage to a structure, after a given level of earthquake is regulated within many modern seismic codes. The intensity of the event is defined as a probabilistic value, such as 10% exceedance probability in 50 years and a structure is classified based on its type of usage, such as a school, a hospital or a residential building. These classes of structures i.e. *structures that are heavily populated for a short duration* or *structures that contain hazardous materials*, have their own performance targets to meet for different levels of shaking.

The performance of a structure under earthquake loading is classified under 3 states in the current Turkish seismic code, [20]. These are *HK*, structures that are safe to use immediately after the seismic event, *CG*, structures that do not pose a hazard in loss of life, and *GÖ*, structures that are collapse prevented only. These global performance targets are associated with properties such as predetermined numbers for maximum contribution ratios of members at different levels of damage (in each storey and/or in the structure as a whole).

The level of damage at the material level is determined from the classification of each region in member elasto-plastic deformation curves (such as moment-curvature diagrams). The classes of member level damage vary between *minimum damage* to *collapse zone*.

The approach described above is known as a performance based approach. If, the approximated behavior of the structure is known via a fine FEM, the evaluation of damage in terms of seismic codes become trivial with specific performance provisions in the codes for specific analysis types. Assessment or design depend on two different approaches, one is force or capacity based, where $\frac{demand}{capacity}$ parameters are checked for members, and the other is the displacement based approach, where displacement

demand is checked against the ductility available.

A simplified approach to computation of both the force and the ductility limitations on the structure is through a linear analysis (i.e. through a linear time history analysis). A linear analysis may become especially beneficial, where there is a lack information with regard to nonlinearities involved. In order to circumvent the lack of nonlinearity information, conservative assessment (or design) guidelines are available in most of the modern seismic codes.

Given the real loading time series of the future earthquake, one could compute a realistic behavior of the structure with Nonlinear Time History Analysis (NTHA) that has nonlinearities and the soil-structure interaction correctly modeled. Lacking the luxury of the records from the future, one could select a set of earthquake records that are in similarity to the expected event through Peak Ground Acceleration (PGA) and distance to epicenter and/or other properties. It is also possible to follow simplified approaches such as a push over analysis (Nonlinear static).

The major problem with conventional push over analysis is the fact that it assumes the first mode to dominate the behavior of the structure (not recommended for structures with a first period greater than one second in ATC-40 [46]). Methodologies, incorporating higher modes into push over analysis are developing. Examples can be found in [47–49].

The most reliable analysis method currently available is NTHA. A reliable NTHA needs to account for several nonlinearities and the soil-structure interaction (mandatory for some soil types in [20]). While some of the nonlinear aspects such as plastic hinges of members are well documented, others such as the effect of masonry infill walls are not entirely agreed upon and are being investigated. The assumptions on the location and number of the plastic hinges is another important dispute. Unwarranted non-ductilities, such as shear failures at the member level, can seriously undermine the reliability of a NTHA. For this purpose, Turkish seismic code [20], dictate that reliable information needs to be gathered for the structure in question prior to an assessment.

This information gathering is provisioned depending on the "information level" of the specific structure, such as "limited information" or "extensive information". Where necessary, it is required that the concrete clear covers are stripped and the reinforcement detailing is examined for proper modelling of the structure. The amount and type of such investigative measures depend on the "information level" discussed above.

Most modern seismic codes share similar performance based seismic evaluation principles, and are directly effected by the new findings from the research on open questions (i.e. effect of masonry walls). Therefore, engineering practices, code provisions and research projects go in parallel and continue to change on a global scale, for improvement of seismic hazard mitigation.

With regard to ETA-B building considered in this thesis, the lack of steel reinforcement information forces the analysis type to become a linear one. It is also important to note that the non-ductile behavior assumable for a 1977 building, designed by the 1975 earthquake code, restricts the definitions of the ultimate curvatures available per element, since the assumption of any noteworthy ductility is under credible questioning.

5.2. Linear Time History Analysis

The study in [21] is utilized heavily for earthquake record selection. In [21], six plausible major earthquake scenarios for the İstanbul region is elaborated. The distances of the portrayed faults to the ETA-B building and the PGA values computed for the most severe earthquake scenario in [21] have been utilized to determine a set of 18 earthquakes for linear time history analysis. PGA values mentioned are municipality specific. However, ETA-B building is close to the borders of both Beşiktaş and Sarıyer municipalities. The calculated PGA values for Beşiktaş and Sarıyer are 0.34 g and 0.23 g, respectively. The distances of ETA-B building to the faults considered in [21] are 26.36 km at nearest and about 133 km at its farthest.

A selection of 18 records are obtained from free field sensors with consideration

of the above PGA values and fault distances. These are listed in Table 5.1.

Table 5.1. Earthquake Records Selected.

No.	**Earthquake**	**Date**	**PGA**	**M**	**Distance**	**Source**
1	Chi-Chi, Taiwan	20.09.1999	0.21 g	7.6	19.9 km	PEER
2	Gölcük, Kocaeli	17.08.1999	0.37 g	7.4	46.0 km	TR-KYH
3	Cape Mendocino	25.04.1992	0.20 g	7.0	26.5 km	PEER
4	Loma Prieta	18.10.1989	0.26 g	6.9	24.5 km	PEER
5	Hawaii	15.10.2006	0.24 g	6.7	**56.7** km	CESMD
6	San Fernando	09.02.1971	0.20 g	6.6	**34.9** km	CESMD
7	Eastern Honshu, Japan	11.04.2011	0.35 g	6.6	**24.8** km	NIED
8	Big Bear	28.06.1992	0.23 g	6.5	**39.4** km	CESMD
9	Coalinga	02.05.1983	0.18 g	6.4	24.8 km	PEER
10	Parkfield	28.09.2004	0.35 g	6.0	**31.2** km	CESMD
11	Erzurum	30.10.1983	0.18 g	6.0	22.6 km	TR-KYH
12	Whittier Narrows	01.10.1987	0.26 g	6.0	21.4 km	PEER
13	Ceyhan, Adana	27.06.1998	0.28 g	5.9	40.0 km	TR-KYH
14	Balıkesir	18.07.1979	0.28 g	5.2	28.9 km	TR-KYH
15	Düzce	26.08.2001	0.19 g	5.1	22.8 km	TR-KYH
16	Gümüşhane	12.08.1985	0.17 g	4.9	80.4 km	TR-KYH
17	Inglewood	17.05.2009	0.21 g	4.7	**25.1** km	CESMD
18	Hatay	30.06.1981	0.16 g	4.7	25.0 km	TR-KYH

PEER [50], TR-KYH [51], CESMD [52] and NIED [53] databases are utilized in order to obtain the earthquake record collection (NIED database is utilized via records donated to one of partner databases of CESMD, namely COSMOS [54]). The distances in Table 5.1 are Joyner-Boore distances except where they are bold. The bold measurements refer to epicentral distance to the recording station.

The minimum and maximum values of PGAs in Table 5.1 are 0.16 g and 0.37 g,

with an average of 0.24 g, which can be thought to mimic the worst-case scenario PGAs for Sarıyer region in [21]. Records also range from 19.9 km to 80.4 km for distances with an average of 33.1 km which is close to the distance ETA-B is from the nearest fault involved in [21]'s scenarios.

These earthquakes have been used to obtain the instantaneous story drifts of both the model updated and non-updated FEMs. The analysis type applied is linear time history analysis due to both the non-ductile behavior assumed and the lack of steel reinforcement information, as stated in Section 5.1. These instantaneous story drifts are then post-processed to obtain the maximum drifts during the earthquakes. These values are then adopted as a basis for a gaussian distribution to evaluate the differences in the probabilities of exceedance of certain storey drift ratios to compare the models and distinguish the effect model updating had on the initial FEM.

For this purpose, linear time history analysis load cases in the SAP2000 program have been defined. From the two possible calculation options: direct integration and modal, modal time history analysis have been selected to be utilized with Ritz mode shapes. These Ritz mode shapes are calculated with a target modal mass participation ratio of 99% in the three acceleration loading directions, X,Y and Z.

It shall be noted that the P-Delta effects are ignored and the Young's moduluses found from the model updating relate to a curvature range only suitable for operational (service) conditions. Therefore, the analysis results shall be reviewed only as a comparison of the updated and non-updated models.

In order to capture the maximum story drift (with respect to story below) at a given story, four corner points at each floor (the top floor's dimensions are being referred to as floor in general) have been selected for extracting time history outputs. If rigid diaphragm behavior at each floor is assumed, then there are two motions that can contribute to the story drift at any given time, namely, rigid body translation and rigid body rotation. Since, the rigid body translation will produce same displacement vectors for the whole floor, it is easy to visualize that any maximum drift at a floor is

going to occur at one of the corner joints. At each time instant the maximum drift is calculated (an absolute value calculated from X and Y relative displacements) as the maximum value obtained from these four corner joints.

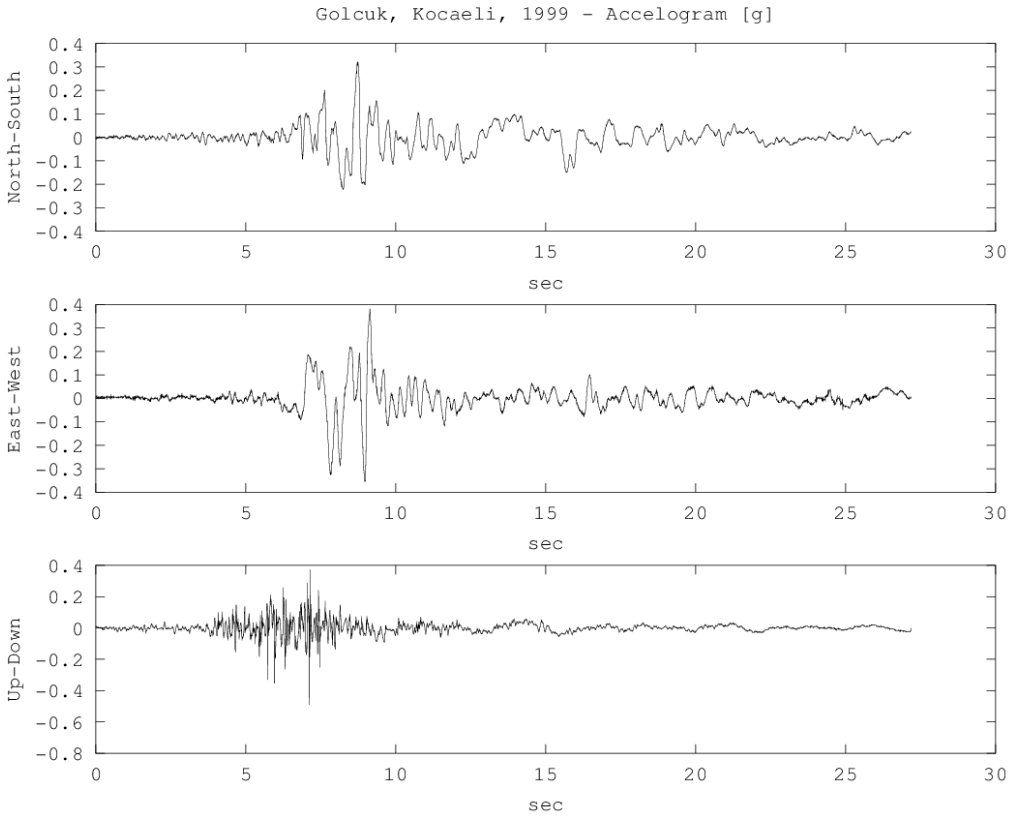

Figure 5.1. Gölcük, Kocaeli 1999 Earthquake Record.

As an example, Figure 5.2 shows the instantaneous maximum drift ratios, maximum of $\sqrt{(drift_x(t))^2 + (drift_y(t))^2}$ from any corner of any floor, of the two models under the Gölcük 1999 earthquake record shown in Figure 5.1.

With a few exceptions where story drift of Level 5 reaches relatively high values for a short duration, the maximum story drifts are generally occurring at Level 0 (above Level -1, which is the foundation level). This can be used to conclude that the deformed shape of both models have a tendency towards the general deformation scheme of a frame resistant structure rather than a structure whose motion is dominated by structural walls.

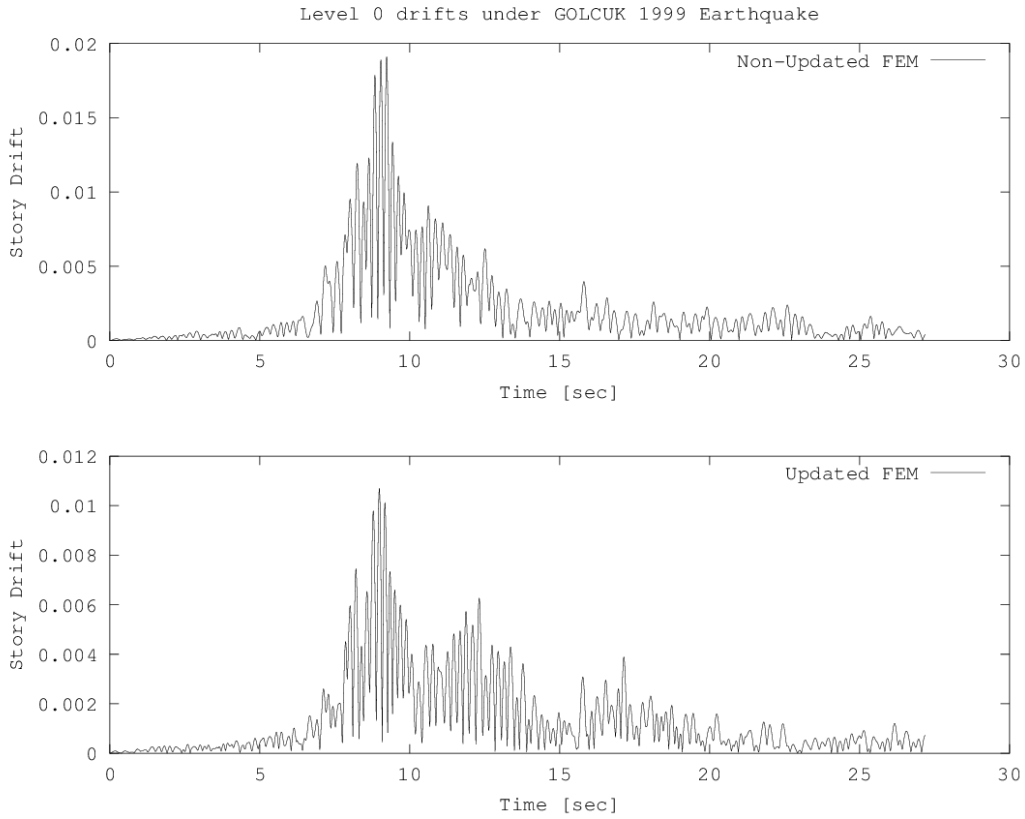

Figure 5.2. Maximum Drift Response of Updated and Non-updated FEMs to Gölcük Earthquake.

It is also noteworthy to realize the distinct effect of model updating in Figure 5.2, where the updating have reduced the maximum drift ratio from orders of 2% to 1%.

To elaborate on these 1% and 2% drift ratios, we can re-consider the fictitious column section in Section 4.4. Assuming its behavior as linear up to 1,300 kNm of moment under 723 kN of compression, we can assume $M = EI \times \psi$. For a fixed-fixed boundary condition, this leads to $D = \psi_{max} \times \frac{L}{6}$, where D is the storey drift ratio.

From this relationship one could compute the storey drift at yield moment for the section, 0.67%. Realizing that, the section chosen is the most dominant column section at Level 0 and comparing the dimensions of other sections to the one investigated, it is easy to realize most of the columns at this first level will form plastic hinges at or below 1% storey drift.

As for 2% storey drift ratio, the modern Turkish seismic code, [20] prohibits storey drift ratios higher than 2% in section 2.10.1.3, since they are viewed as excessive.

6. CONCLUSION AND RECOMMENDATIONS

In earthquake prone areas, assessing the safety of existing structures is a vital concern. The primary tool available to the modern civil engineer to solve this problem is almost invariably a FEM. However experienced the engineer or detailed the model, it is not possible to ensure the behavioral similarity between the simulations and the real life events. Therefore, the shortcomings of this dependency is equally translated as a need for conservatism in the results of any assessment work.

In SHM, since the actual dynamic behavior of the real world structure is monitored and the modal information is extracted from such data, the immediate answer to the how far off a FEM is from reality is readily answered. Still, the fundamental value of SHM is the access to a feedback and improvement mechanism for the dependability of the FEM, namely through model updating.

The type of analysis (linear/nonlinear, static/dynamic) following the acquirance of an improved FEM, does not introduce additional constraints on SHM's utilization. Assuming that the trade between an *unknown degree of conservatism* and *a measurable degree of correspondance* (via MAC values and frequencies), at the cost and effort required for a SHM study is an obvious choice. It shall be especially desirable where the decision to demolish, retrofit or approve a building for safety is to be made.

ETA-B building is used as a means for distinguishing the effects of availability of SHM, as discussed above. This is aimed to be achieved by demonstrating the difference between the storey drift probability distributions in the expected İstanbul earthquake. The results show the possibility of a decision change from demolishing to retrofitting. It shall be noted that, ETA-B building is actually retrofitted and also expanded, without the use of SHM in the decision making process. However, considering the land availability and the need for new classrooms in the campus, the decision is likely to involve more parameters than the ones in this study. For these reasons, no direct links to the results of this thesis and the decisions taken by the University administration

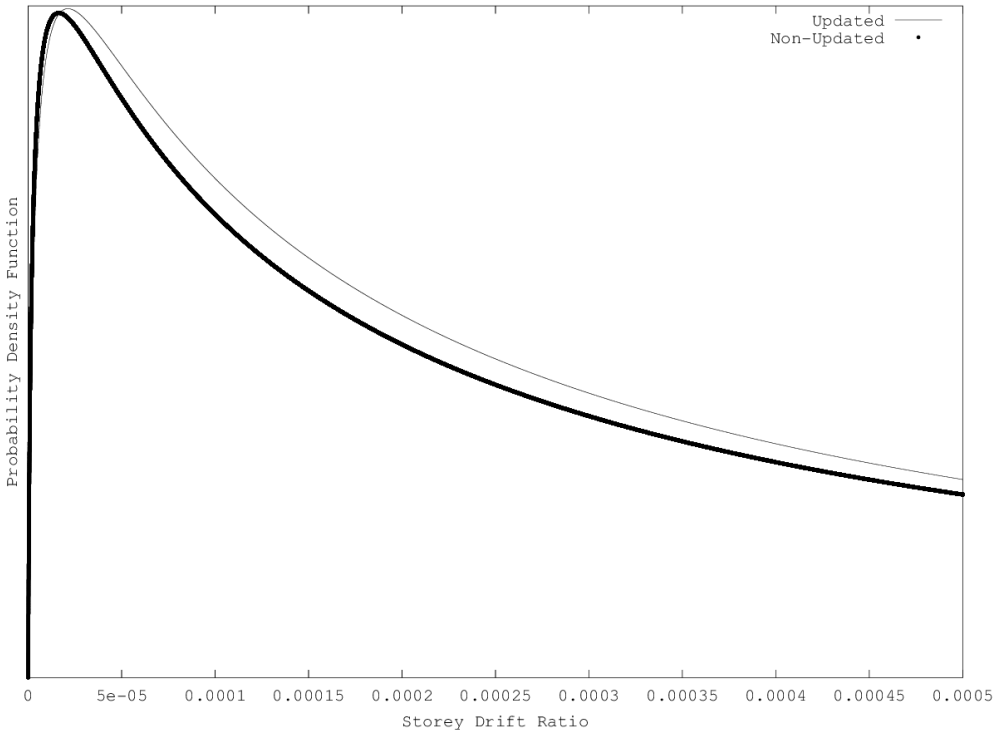

Figure 6.1. Lognormal Distribution for Maxium Storey Drift Ratio.

can be constructed.

Figure 6.1 shows the lognormal distribution obtained by the maximum drift ratios under each earthquake record. The values used are absolute drift ratios, calculated from the maximum of $drift(t)$ of all floor corners, where

$$drift(t) = \sqrt{(drift_x(t))^2 + (drift_y(t))^2} \tag{6.1}$$

Assuming a lognormal distribution for the PGA levels and neglecting the variability that could be introduced for the same PGA level in response, (since, the Probability Distribution Function, PDF of an attenuation on the frequency content given the PGA would otherwise be necessary) a lognormal distribution is generated for the mean and standard deviation of the maximum absolute drift ratios. Table 6.1 shows a comparison between the results computed for model updated and non-updated FEMs. It can be seen that after model updating, the probability of exceedance of 1% story drift and 2%

Table 6.1. Statistics of Maximum Drift Ratios and Exceedance Probabilities.

	Updated FEM	**Non-Updated FEM**
Average	0.38%	0.52%
Standard Deviation	0.38%	0.61%
Probability of Exceeding 1% Drift	15%	19%
Probability of Exceeding 2% Drift	9%	11%

story drift fall by 18% and 23%, respectively. Cosidering the elaboration in Section 5.2 concerning the meaning of these drift levels for the example column section in Section 4.4, it is possible for these differences to tip the balance for the decision to be made in either retrofitting or demolishing, if the feasibility study to be performed is sensitive to a change of almost 20% in expected performance. Therefore, compared to safety and monetary gains or losses such a decision refers to, the cost and effort required for structural health monitoring can be said to be negligible.

6.1. Recommendations For Future Studies/Applications

The intelligence gathering process prior to building an initial FEM, is perhaps one of the most important stages. For any new researcher, it is advised with upmost importance to try to diminish the addition of new information about the structure, location, code of the day and other concerns as throughly as possible. One of the key subjects to consider at this stage is the previous studies done on the structure or near the structure. I was able to obtain archived hand drawings, along with Computer Aided Design (CAD) drawings from a previous thesis research. However, I truly regret not insisting on obtaining direct structural data from the construction company that has finished the retrofitting process, since the project requires them to obtain steel reinforcement information through stripping of columns and concrete strength values. Had this been done, the scope of the thesis could easily be extended to include NTHA, which is much more desirable.

The second issue is that if the researcher has the opportunity to collect data themselves, it shall be remembered that the design of the allocation of the sensors in the tests will be a major limiting factor in the identification and later in the model updating processes. It is seen on the data that was available in this thesis that, night time records are generally higher quality than that of day time records, and the data collected via sensors whose data cables are prevented from moving (via taping to contact surface) have much less jumps in their records.

On a third and final remark, if the structure has a configuration that will cause considerable amount of overall volume overlap of the connecting frames and areas, there is every possibility that the mass of the structure is to be estimated higher than it actually is. Therefore, it is advised to limit the error that could be contributed due to mass overlaps in the model as much as possible.

APPENDIX A: MATHEMATICAL PRELIMINARIES

Some mathematical fundamentals will be covered in this appendix, to allow the flow of the discussions in the thesis to be more fluid, and unhindered by the formulations and proofs to be presented here. These concepts are then to be referred to in the thesis without rigorous explanation.

A.1. Fourier Transform Derivation and Convolutions

Some trigonometric identities that will be used

$$sin(mx)cos(nx) = \frac{1}{2}\{sin([m+n]x) + sin([m-n]x)\} \tag{A.1}$$

$$cos(mx)cos(nx) = \frac{1}{2}\{cos([m+n]x) + cos([m-n]x)\} \tag{A.2}$$

$$sin(mx)sin(nx) = \frac{1}{2}\{cos([m+n]x) - cos([m-n]x)\} \tag{A.3}$$

$$cos(\theta) = cos(-\theta) \tag{A.4}$$

$$sin(\theta) = -sin(-\theta) \tag{A.5}$$

$$e^{i\theta} = cos(\theta) + i \times sin(\theta) \tag{A.6}$$

$$sin(u \pm v) = sin(u)cos(v) \pm cos(u)sin(v) \tag{A.7}$$

$$cos(u \pm v) = cos(u)cos(v) \mp sin(u)sin(v) \tag{A.8}$$

For equations below $-\pi \leq x < \pi$, unless stated otherwise.

by Equation A.4

$$\int_{-\pi}^{\pi} sin(nx)\,\mathrm{d}x = 0 \tag{A.9}$$

by Equation A.5

$$\int_{-\pi}^{\pi} cos(nx)\,\mathrm{d}x = 0, \quad n \in Z \tag{A.10}$$

by Equation A.3 and A.10

$$\int_{-\pi}^{\pi} sin^2(nx)\,\mathrm{d}x = \pi, \quad 2n \in Z \tag{A.11}$$

by Equation A.2 and A.10

$$\int_{-\pi}^{\pi} cos^2(nx)\,\mathrm{d}x = \pi, \quad 2n \in Z \tag{A.12}$$

by Equation A.1 and A.9

$$\int_{-\pi}^{\pi} sin(mx)cos(nx)\,\mathrm{d}x = 0 \tag{A.13}$$

by Equation A.3, A.10 and A.11

$$\int_{-\pi}^{\pi} sin(mx)sin(nx)\,\mathrm{d}x = \begin{cases} 0 & \text{if, } m \neq n, \quad m \in Z, \quad n \in Z \\ \pi & \text{if, } m = n, \quad 2n \in Z \end{cases} \tag{A.14}$$

by Equation A.10 and A.12

$$\int_{-\pi}^{\pi} cos(mx)cos(nx)\,\mathrm{d}x = \begin{cases} 0 & \text{if, } m \neq n, \quad m \in Z, \quad n \in Z \\ \pi & \text{if, } m = n \neq 0, \quad 2n \in Z \\ 2\pi & \text{if, } m = n = 0 \end{cases} \tag{A.15}$$

by L'Hopital

$$\lim_{x \to 0} sinc(x) = 1 \tag{A.16}$$

by Equation A.6 and A.16

$$\int_{-\pi}^{\pi} e^{imx}e^{-inx}\,\mathrm{d}x = \begin{cases} 0 & \text{if, } m \neq n \\ 2\pi & \text{if, } m = n \end{cases} \tag{A.17}$$

It can be seen from Equations A.13,A.14 and A.15 that *sine* and *cosine* functions are orthogonal functions. They form a basis for the following function space for 2π periodic functions. (n denotes a n^{th} degree Fourier polynomial)

$$F_n(x) = a_0 + \sum_{k=1}^{k=n} \{a_k cos(kx) + b_k sin(kx)\} \quad k, n \in N, \quad k \in [1, n] \tag{A.18}$$

where,
by Equation A.9 and A.10

$$a_0 = \frac{1}{2\pi} \int_{-\pi}^{\pi} F_n(x)\,\mathrm{d}x \quad k \in Z \tag{A.19}$$

by Equation A.10, A.13 and A.15

$$a_k = \frac{1}{\pi} \int_{-\pi}^{\pi} F_n(x) cos(kx)\,\mathrm{d}x \quad k \in Z \tag{A.20}$$

by Equation A.9, A.13 and A.14

$$b_k = \frac{1}{\pi}\int_{-\pi}^{\pi} F_n(x)sin(kx)\,\mathrm{d}x \quad k \in Z \tag{A.21}$$

For below equations the following variable conversion applies, $x = \frac{2\pi}{T} \times t$, therefore $-T/2 \leq t < T/2$

$$f_n(t) = c_0 + \sum_{k=1}^{k=n}\{d_k cos(k\frac{2\pi t}{T}) + e_k sin(k\frac{2\pi t}{T})\} \quad k, n \in N, \quad k \in [1, n] \tag{A.22}$$

where

$$c_0 = \frac{1}{T}\int_{-T/2}^{T/2} f_n(t)\,\mathrm{d}t \quad k \in Z \tag{A.23}$$

$$d_k = \frac{2}{T}\int_{-T/2}^{T/2} f_n(t)cos(k\frac{2\pi t}{T})\,\mathrm{d}t \quad k \in Z \tag{A.24}$$

$$e_k = \frac{2}{T}\int_{-T/2}^{T/2} f_n(t)sin(k\frac{2\pi t}{T})\,\mathrm{d}t \quad k \in Z \tag{A.25}$$

where

$$f_n(t) = f_n(\frac{Tx}{2\pi}) = F_n(x) \tag{A.26}$$

It also follows from Equation A.17 and A.6 that,

$$f_n(t) = \sum_{k=-n}^{k=n} f_k e^{i\theta_k} \quad where, \theta_k = k \times \frac{2\pi t}{T} \quad k, n \in N, \quad k \in [-n, n] \tag{A.27}$$

where

$$f_k = \frac{1}{T}\int_{-T/2}^{T/2} f_n(t)e^{-i\theta_k}\,\mathrm{d}t \tag{A.28}$$

Let t continuous variable be discretised by $t_j = j \times \frac{T}{N}$ then $-N/2 \leq j < N/2 \quad j \in Z$ and $j = -N/2, -N/2+1, ...N/2-1$, and since $e^{i\frac{2\pi}{N}}$ has N roots ($1^{1/N}$), we can form a basis for the function space with N independent terms in the summation. (This effectively replaces n of $f_n(t)$ with N roots of $e^{i\frac{2\pi}{N}}$)

$$f(t_j) = \sum_{k=-N/2}^{k=N/2-1} f_k e^{iw_k t_j} \tag{A.29}$$

$$f_k = \frac{1}{N}\sum_{j=-N/2}^{j=N/2-1} f(t_j)e^{-iw_k t_j} \tag{A.30}$$

where $w_k = k \times \frac{2\pi}{T} \quad t_j = j \times \frac{T}{N}$

The Equations A.29 and A.30 together form the pair known as *Discrete Fourier Transform*. Please note that, if we have started with the time variable as $0 \leq t < T$ and $t = \frac{Tx}{2\pi} + \frac{T}{2}$, we would have reached the same conclusion with the minor changes being $k = 0, 1, 2, ..., N-1$ and $j = 0, 1, 2, ..., N-1$.

If, at Equations A.27 and A.28, we turn discrete $k \in [-n, n]$, $k \in Z$ into continuous k, let T go to infinity, and we let $w = k \times 2\pi/T$ and $f(w) = T \times f_k$, we will get to *Fourier Integral Transform* equations.

$$f(t) = \frac{1}{2\pi}\int_{-\infty}^{\infty} f(w)e^{iwt}\,\mathrm{d}w \tag{A.31}$$

$$f(w) = \int_{-\infty}^{\infty} f(t)e^{-iwt}\,\mathrm{d}t \tag{A.32}$$

Suppose we have a function $f(t)$ such that, (The following methodology is attained from [55])

$$f(t) = \begin{cases} e^{at} & if, t \leq 0 \\ e^{-at} & if, t > 0 \end{cases} \qquad a > 0 \tag{A.33}$$

Then

$$f(w) = \frac{2a}{a^2 + w^2} \tag{A.34}$$

Now, let us suppose we have the following differential equation to solve.

$$-\ddot{u}(t) + a^2 u(t) = f(t), \quad -\infty < t < \infty, \quad u(-\infty) = u(\infty) = 0 \tag{A.35}$$

Taking Fourier integral transforms of both sides,

$$w^2 u(w) + a^2 u(w) = f(w) \tag{A.36}$$

$$u(w) = \frac{f(w)}{a^2 + w^2} \tag{A.37}$$

If we had $f(t) = \delta(t)$, $f(w)$ would have been 1 and $u(w)$ would have been $\frac{1}{a^2+w^2}$. By Equation A.33 and A.34 we can see that, then $u(t)$ would have been equal to $G(t)$ below.

$$G(t) = \begin{cases} \frac{e^{at}}{2a} & if, t \leq 0 \\ \frac{e^{-at}}{2a} & if, t > 0 \end{cases} \qquad a > 0 \tag{A.38}$$

G(t) is known as *the Green's Function.*

Since, we can decompose $f(t)$ into infinitely many impulses equal to function's

own value at the specific impulse location, we can state that;

$$f(t) = \int_{-\infty}^{\infty} f(x)\delta(t-x)\ \mathrm{d}x \tag{A.39}$$

Stated otherwise, $f(t)$ is its own convolution with dirac delta function in time space, where $*$ stands for convolution in the equation below (non-cyclic).

$$f = f * \delta \tag{A.40}$$

Since, for every $\delta(t-t_0)$ impulse of $f(t)$ on time domain, there exists a corresponding $G(t-t_0)$ function for $u(t)$, (linear time invariant) we can state the same combination of $f(x)$ coefficients that make $f(t)$ out of $\delta(t-t_0)$ impulses, will make $u(t)$ out of $G(t-t_0)$ functions.

$$u(t) = \int_{-\infty}^{\infty} f(x)G(t-x)\ \mathrm{d}x \tag{A.41}$$

$$u = f * G \tag{A.42}$$

We also know from the case where $f(t)$ is equal to just one $\delta(t)$ impulse, $u(w)$ is equal to $G(w)$, since $\delta(w) = 1$ we can manipulate to get $u(w) = f(w)G(w)$, for $f(t) = \delta(t)$, and since we have Linear Time Invariant (LTI) property we can extend this to any $f(t)$ to get $u(w) = f(w)G(w)$. Then we have,

$$\begin{aligned} f = f * \delta \qquad & f(w) = f(w)\delta(w) \\ u = f * G \qquad & u(w) = f(w)G(w) \end{aligned} \tag{A.43}$$

Which basically states that, a convolution in time space is a multiplication in frequency space (Although, it is not proven here, the reverse is also true.).

A.2. Random Data

This section contains preliminaries on random data for the discussion on response to random vibrations in Section 2.1, and signal processing in the Appendix B.

For demonstration purposes, let us be interested in the probable air pressure under a given bridge design to be assessed and let us call the random process of real time air pressure distribution under any bridge of this design as $x(t)$. For different bridges of the same design built on different terrains we would have different air pressure distributions for $-\infty < t < \infty$ such as $x_1(t), x_2(t), ...$ where $x_i(t)$ is called a *sample function* and the collection of all sample functions is called the *ensemble*.

For random-stochastic processes such as these, we can not employ a deterministic equation to predict the exact value for the next occurrence, but we can proceed with the aim of obtaining a statistical model to define the physics. This statistical information is obtained from the correlation functions for the processes.

In below equations $x(t)$, $U(t)$, $F(t)$ are real valued functions of a real variable and they have zero mean values, in line with the discussions on accelerations and forces in Chapter 2.

$$R(t,\tau) = E[x(t)x(t+\tau)] = \frac{1}{n}\sum_{i=1}^{n} x_i(t)x_i(t+\tau) \tag{A.44}$$

Where n is the number of sample functions in the ensemble, Equation A.44 gives the *autocorrelation* function for τ amount of time delay between $x(t)$ values.

If, the processes conforms to the statistical model where the probability distribution function, PDF does not change over time, such a process is called a *stationary random process*. Consequently for an unchanging PDF, $E[x(t)x(t+\tau)]$ is independent of t and $R(t,\tau) = R(\tau)$ is a function of τ, time delay only.

An *ergodic* process is a type of stationary random process for which, a single sample function is representative of the whole ensemble for statistical purposes. For such a random process, Equation A.44 reduces to the following.

$$R(\tau) = \lim_{T\to\infty} \frac{1}{T} \int_{-T/2}^{T/2} x(t)x(t+\tau)\ \mathrm{d}t \tag{A.45}$$

Where $x(t)$ now stands for the single sample function of the stationary and ergodic random process. We can also calculate the cross-correlation of two different sample functions (or cross-correlation of two different processes, something we might want to do for example if the processes are related in a cause and effect relationship), as in Equation A.46.

$$R_{UF}(\tau) = \lim_{T\to\infty} \frac{1}{T} \int_{-T/2}^{T/2} U(t)F(t+\tau)\ \mathrm{d}t \tag{A.46}$$

$$S_{UF}(w) = \frac{1}{2\pi} \int_{-\infty}^{\infty} R_{UF}(\tau)e^{-iw\tau}\ \mathrm{d}\tau \tag{A.47}$$

Where $S_{UF}(w)$ is the cross power spectral density, which is the Fourier integral transform of $\frac{R(\tau)}{2\pi}$ for stationary processes (This result can be obtained as a cross-correlation extension to the Wiener-Khinchin Theorem.).

The cross-correlation theorem, which will be used in deriving the response of a structure to random vibrations, states that;

$$F\{R_{fg}(\tau)\} = \overline{F\{f(t)\}}F\{g(t)\} \tag{A.48}$$

Where in Equation A.48, the $F\{\}$ stands for Fourier transform, $\overline{x}$ stands for complex conjugate of x, $f(t)$ and $g(t)$ are complex valued functions of real variable t and the definition of $R_{fg}(\tau)$ is changed accordingly as,

$$R_{UF}(\tau) = \int_{-\infty}^{\infty} \overline{U(t)}F(t+\tau)\ \mathrm{d}t \tag{A.49}$$

Since for real valued $U(t)$, $U(t) = \overline{U(t)}$ cross-correlation theorem applies to our $R(\tau)$ definition as well. If $U(t) = F(t)$ the cross-correlation theorem reduces to Wiener-Khinchin Theorem, which we can then extend for the $R_{UF}(\tau)$ vs. $S_{UF}(w)$ relationship in Equations A.46 and A.47.

APPENDIX B: SIGNAL PROCESSING

The signal we obtain from civil engineering structures is usually the acceleration response, since it is not practical to obtain displacement or velocity readings from large structures. Before we can extract structural information from the data, it shall be subject to signal processing to become usable for system identification.

First task is to relieve the data off of jumps like the one in Figure B.1. These may occur due to voltage jumps in the data collection set up, or physical impacts to the sensor.

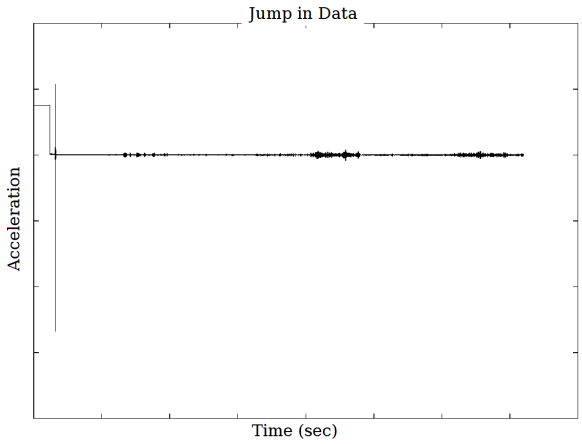

Figure B.1. Jump in Time Series Data.

Next, it is needed to detrend the data, trending may occur due to various causes which are not fully controllable during data collection, such as the glue fixing the sensor to the structure might be loosening with the tension applied from the data cable. Figure B.2 shows a trending data series.

Next, we proceed to solve analogue to digital conversion problems, namely, aliasing, noise, leakage and spilling.

Visualising the aliasing problem in time space in a simple example, Figure B.3

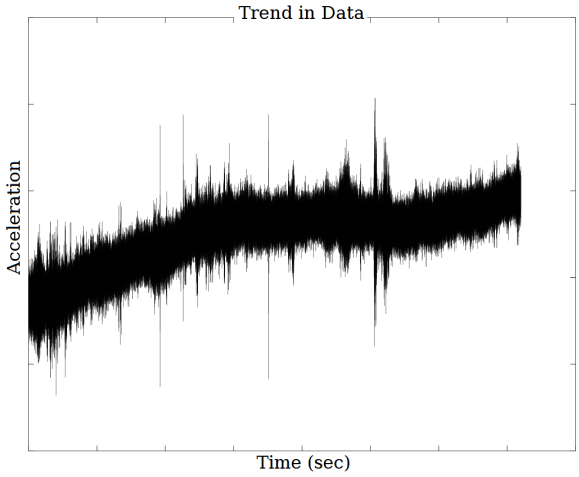

Figure B.2. Trend in Time Series Data.

shows three time signals, one of them is the all zero signal, and the other two are sine waves of different frequencies. If the sampling is made for all three of these signals with the time step, dt shown in the figure, all of the data samples will be zero, thus one can not determine by this sampling, which of the three or infinitely many more other time series, do this data actually belong to.

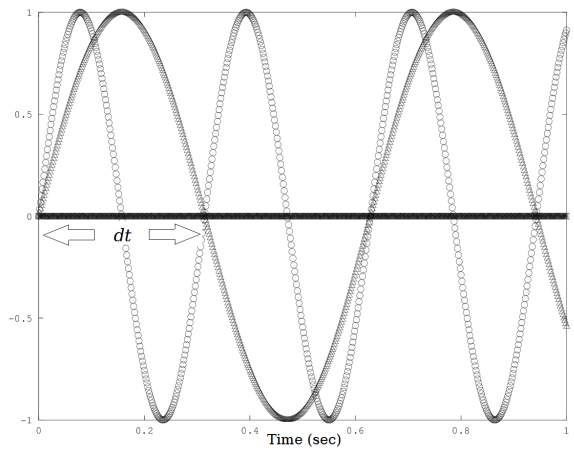

Figure B.3. Aliasing Signals in Time Series.

To demonstrate mathematically, suppose we have a T periodic analogue signal

$f(t)$, sampled at N equal time intervals covering T amount of time, such that,

$$\begin{aligned}
T, &\quad \text{period of } f(t)\\
SF = N \times 2\pi/T, &\quad \text{sampling frequency in rad-Hz}\\
-T/2 \leq t < T/2, &\quad \text{continuous time space}\\
-SF/2 \leq w < SF/2, &\quad \text{continuous frequency space}\\
dt = T/N, &\quad \text{time step}\\
dw = 2\pi/T, &\quad \text{frequency step}\\
j = -N/2, -N/2+1 ... N/2-1, &\quad \text{time index}\\
k = -N/2, -N/2+1 ... N/2-1, &\quad \text{frequency index}\\
t_j = j \times dt, &\quad \text{discrete time space}\\
w_k = k \times dw, &\quad \text{discrete frequency space}
\end{aligned}$$

Looking back to discrete Fourier transform equations, Equation A.29, and Equation A.30, since we can show the following,

$$e^{iw_k t_j} = e^{ik\frac{2\pi}{T}j\frac{T}{N}} \tag{B.1}$$

$$= e^{i(k\frac{2\pi}{T}+m\frac{2\pi N}{T})j\frac{T}{N}}, m \in Z \tag{B.2}$$

$$(e^{i2\pi})^{kj} = (e^{i2\pi})^{(k+mN)j} \tag{B.3}$$

we can state that, at this sampling rate we have aliasing (shown below as $\equiv$) of the below frequencies for any k.

$$k \equiv k + mN \tag{B.4}$$

$$k\frac{2\pi}{T} \equiv k\frac{2\pi}{T} + mN\frac{2\pi}{T} \tag{B.5}$$

$$w_k \equiv w_k + m \times SF \tag{B.6}$$

So, if the analogue signal has components of frequencies outside $-SF/2 \leq w < SF/2$ range, they will show up in $-SF/2 \leq w_k < SF/2$ discrete frequency range by adding

their f_{k+mN} to f_k and will thereby distort f_k value.

There are two ways used in conjunction or separately to reduce aliasing; analogue anti-aliasing filters, and oversampling of the signal. Analogue anti-aliasing filters are hardware equipments designed to separate $-SF/2 \leq w < SF/2$ range prior to sampling. As a trivial example, a glass prism separating white light into its colors can be thought of as an analogue filter. High quality analogue filters are expensive and just like digital filters, they are subject to *leakage* errors, from the roundness of the filter's frequency spectra at the cut off frequencies.

Oversampling allows the $-SF/2$ to $SF/2$ range to widen to a level such that the nyquist frequency is way above the maximum frequency of interest to us. Thus, the amount of native frequencies in the signal that can alias on the frequencies of interest will reduce. This will also allow for a cheaper analogue anti aliasing filter to be used since the demand from the filter will be reduced. Oversampling also frees the frequency range of interest from leakage errors (errors that are caused by imperfections in the filter are meant here, the leakage error due to periodicity errors that originate from segmenting the data into pieces is resolved by windowing functions), since these will be occurring close to the cut-off frequencies of the filter and one can set cut-off frequencies high enough to protect frequency content of interest. This is possible due to the fact that $\pm SF/2$ values are high enough to permit such cut-off frequencies when oversampling is applied.

Furthermore, the spilling errors caused by the inability of the discrete frequency space w_k to represent every point on continuous w, will be reduced by oversampling, since w_k will be denser.

As in many other applications, the acquired data are contaminated with noise. In ambient vibration testing, the noise is the input to the structure we depend on to produce the output containing the structural information, but on the other hand, the high frequency components of the response are not wanted since they can not contribute valuable information on the structure, whose modal frequencies are at lower values.

To amplify and extract the structural information we resort to two main tools, windowing and digital filters.

The noise is assumed to be of gaussian white noise under ambient vibration testing. This type of noise has a flat power spectral density, in other words it contains same amount from every frequency level and its time series amplitudes follow a normal probability distribution with zero mean, hence the name gaussian.

Since, the mean value is zero for noise, we chop the acceleration record into pieces to be averaged in order to reduce the adverse effects of noise. But, we want to assure the averaged result to have the same start and end value to fit into our periodicity assumption in Discrete Fourier Transform (DFT), otherwise it is equivalent to having an impulse jump in the data, which would show up in the frequency spectrum as a Fourier transform of a corresponding Green's function, $G(w)$. There are a variety of windowing functions to choose from to do this, that are built to multiply the beginning and the ends with zero, thus making the section start and end with same value, and preserve the information in the signal by smoothly transforming from this zero value to one, for the bulk of the window.

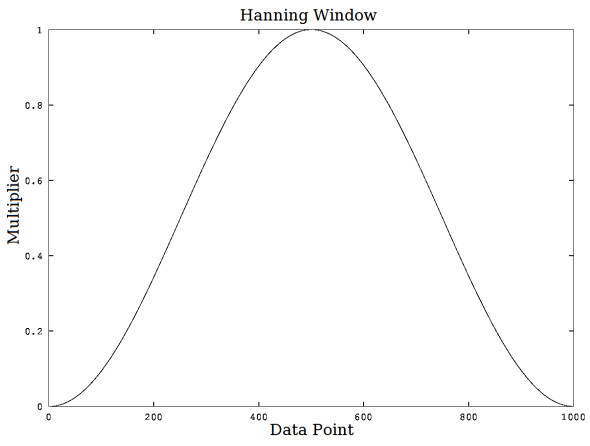

Figure B.4. Hanning Window.

We reduce the unwanted frequency content, usually for civil engineering structures the high frequencies, through application of digital filters before sectioning the

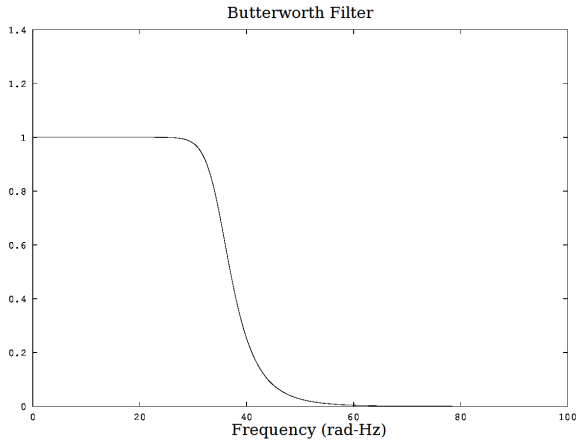

Figure B.5. Butterworth Filter.

data. Therefore, these are not allowed to distort the sectioning, windowing and averaging processes. The choice of the type of digital filter depends on which characteristics of the signal are most valued in the particular application. Figure B.5 shows the butterworth filter with its flat pass band and flat stop band properties apparent. Though, the rounding of at the cut-off frequency suggests a high leakage error, it can be mitigated by an adequate oversampling.

The choices of windowing and filtering procedures and how data sections are treated, is very well established in many types of applications in the literature. It is customary to utilize the Welch procedure for ambient vibration testing [27, 56].

B.1. The Welch Procedure

The following is the summarised methodology of the Welch Procedure [56].

Let $X(j), \quad j = 0, 1, 2, ..., N-1$ be a *stationary* and *second order stochastic* ($E[X^2(j)] < \infty$ for all j), discrete time series such that $E[X] = 0$ (in line with ambient vibration case).

We take D points separated, L data points long sections from $X(j)$ to form

$X_1(j_*), X_2(j_*)...\quad j_* = 0, 1, 2..., L-1$, where $L > D$ so that $X_i(j_*)$ are overlapping one another for a fixed amount (50% is generally used for OMA [27]). Then, we multiply each $X_i(j_*)$ with a window function $W(j_*)$ (Hanning window is generally used for OMA [27]) and take the discrete Fourier transform to get $A_i(w_k)$.

$$I_i(w_k) = \frac{L}{U} \times |A_i(w_k)|^2 \quad where \quad U = \frac{1}{L} \sum_{j_*=0}^{j_*=L-1} W^2(j_*) \tag{B.7}$$

Where, $I_i(k)$ are called the *modified periodograms*. Then the estimate for $X(j)$'s PSD is the average of the modified periodograms.

REFERENCES

1. Cunha, A. and C. Elsa, "Experimental Modal Analysis of Civil Engineering Structures", *Sound and Vibration*, Vol. 40, No. 6, pp. 12–20, 2006.

2. Farrar, C. R. and K. Worden, "An Introduction to Structural Health Monitoring", *Philosophical Transactions: Mathematical, Physical and Engineering Sciences*, Vol. 365, No. 1851, pp. 303–315, 2007.

3. Worden, K., C. R. Farrar, G. Manson and G. Park, "The Fundamental Axioms of Structural Health Monitoring", *Proceedings: Mathematical, Physical and Engineering Sciences*, Vol. 463, No. 2082, pp. 1639–1664, 2007.

4. Yi, W.-J., Y. Zhou, S. Kunnath and B. Xu, "Identification of Localized Frame Parameters Using Higher Natural Modes", *Engineering Structures*, Vol. 30, No. 11, pp. 3082 – 3094, 2008.

5. Altunışık, A. C., A. Bayraktar, B. Sevim and Şevket Ateş, "Ambient Vibration Based Seismic Evaluation of Isolated Gülburnu Highway Bridge", *Soil Dynamics and Earthquake Engineering*, Vol. 31, No. 11, pp. 1496–1510, 2011.

6. Gentile, C. and A. Saisi, "Ambient Vibration Testing and Condition Assessment of the Paderno Iron Arch Bridge (1889)", *Construction and Building Materials*, Vol. 25, No. 9, pp. 3709–3720, 2011.

7. Lardies, J. and M.-N. Ta, "Modal Parameter Identification of Stay Cables from Output-Only Measurements", *Mechanical Systems and Signal Processing*, Vol. 25, No. 1, pp. 133–150, 2011.

8. Magalhães, F., E. Caetano and A. Cunha, "Operational Modal Analysis and Finite Element Model Correlation of the Braga Stadium Suspended Roof", *Engineering Structures*, Vol. 30, No. 6, pp. 1688–1698, 2008.

9. Fukuda, Y., M. Q. Feng and M. Shinozuka, "Cost-Effective Vision-Based System for Monitoring Dynamic Response of Civil Engineering Structures", *Structural Control and Health Monitoring*, Vol. 17, No. 8, pp. 918–936, 2010.

10. Brownjohn, J., P.-Q. Xia, H. Hao and Y. Xia, "Civil Structure Condition Assessment by FE Model Updating: Methodology and Case Studies", *Finite Elements in Analysis and Design*, Vol. 37, No. 10, pp. 761–775, 2001.

11. Wu, J. and Q. Li, "Structural Parameter Identification and Damage Detection for a Steel Structure Using a Two-Stage Finite Element Model Updating Method", *Journal of Constructional Steel Research*, Vol. 62, No. 3, pp. 231–239, 2006.

12. Hashim, H., Z. Ibrahim and H. A. Razak, "Dynamic Characteristics and Model Updating of Damaged Slab from Ambient Vibration Measurements", *Measurement*, Vol. 46, No. 4, pp. 1371–1378, 2013.

13. Satake, N., K. ichi Suda, T. Arakawa, A. Sasaki and Y. Tamura, "Damping Evaluation Using Full-Scale Data of Buildings in Japan", *Journal of Structural Engineering*, Vol. 129, No. 4, pp. 470–477, 2003.

14. Güler, K., E. Yüksel and A. Koçak, "Estimation of the Fundamental Vibration Period of Existing RC Buildings in Turkey Utilizing Ambient Vibration Records", *Journal of Earthquake Engineering*, Vol. 12, No. 2, pp. 140–150, 2008.

15. Oliveira, C. S. and M. Navarro, "Fundamental Periods of Vibration of RC Buildings in Portugal from In-Situ Experimental and Numerical Techniques", *Bulletin of Earthquake Engineering*, Vol. 8, No. 3, pp. 609–642, 2010.

16. Lombaert, G., B. Moaveni, X. He and J. Conte, "Damage Identification of a Seven-Story Reinforced Concrete Shear Wall Building Using Bayesian Model Updating", *Proceedings of the IMAC-XXVII*, 2009.

17. Zonta, D., A. Elgamal, M. Fraser and M. N. Priestley, "Analysis of Change In

Dynamic Properties of a Frame-Resistant Test Building", *Engineering Structures*, Vol. 30, No. 1, pp. 183–196, 2008.

18. Michel, C., P. Guéguen and P.-Y. Bard, "Dynamic Parameters of Structures Extracted from Ambient Vibration Measurements: An Aid for the Seismic Vulnerability Assessment of Existing Buildings in Moderate Seismic Hazard Regions", *Soil Dynamics and Earthquake Engineering*, Vol. 28, No. 8, pp. 593–604, 2008.

19. Boutin, C., S. Hans, E. Ibraim and P. Roussillon, "In-Situ Experiments and Seismic Analysis of Existing Buildings. Part II: Seismic Integrity Threshold", *Earthquake Engineering and Structural Dynamics*, Vol. 34, No. 12, pp. 1531–1546, 2005.

20. *Deprem Bölgelerinde Yapılacak Binalar Hakkında Yönetmelik*, 2007, T.C. Bayındırlık ve İskan Bakanlığı.

21. Gülkan, P., "Expecting the Expected: 1 g Peak Motions in the İstanbul Metropolitan Area", *15th World Conference on Earthquake Engineering*, 2012.

22. *Afet Bölgelerinde Yapılacak Yapılar Hakkında Yönetmelik*, 1975, T.C. Bayındırlık ve İskan Bakanlığı.

23. Wirsching, P. H., T. L. Paez and K. Ortiz, *Random Vibrations : Theory and Practice*, John Wiley & Sons, Inc., New York, NY, USA, 1995.

24. Brincker, R., L. Zhang and P. Andersen, "Modal Identification of Output-Only Systems Using Frequency Domain Decomposition", *Smart Materials and Structures*, Vol. 10, No. 3, pp. 441–445, 2001.

25. Rainieri, C. and G. Fabbrocino, "Automated Output-Only Dynamic Identification of Civil Engineering Structures", *Mechanical Systems and Signal Processing*, Vol. 24, No. 3, pp. 678–695, 2010.

26. Rainieri, C., G. Fabbrocino and E. Cosenza, "Near Real-Time Tracking of Dynamic

Properties for Standalone Structural Health Monitoring Systems", *Mechanical Systems and Signal Processing*, Vol. 25, No. 8, pp. 3010–3026, 2011.

27. Magalhães, F., Á. Cunha, E. Caetano and R. Brincker, "Damping Estimation Using Free Decays and Ambient Vibration Tests", *Mechanical Systems and Signal Processing*, Vol. 24, No. 5, pp. 1274–1290, 2010.

28. Beck, J. L. and L. S. Katafygiotis, "Updating Models and Their Uncertainties. I: Bayesian Statistical Framework", *Journal of Engineering Mechanics*, Vol. 124, No. 4, pp. 455–461, 1998.

29. Butt, F. and P. Omenzetter, "Seismic Response Trends Evaluation via Long Term Monitoring and Finite Element Model Updating of an RC Building Including Soil-Structure Interaction", *Proceedings of the SPIE 8347*, 2012.

30. Bakır, P. G., E. Reynders and G. D. Roeck, "Sensitivity-Based Finite Element Model Updating Using Constrained Optimization with a Trust Region Algorithm", *Journal of Sound and Vibration*, Vol. 305, No. 1, pp. 211–225, 2007.

31. Au, S.-K., "Connecting Bayesian and Frequentist Quantification of Parameter Uncertainty in System Identification", *Mechanical Systems and Signal Processing*, Vol. 29, pp. 328–342, 2012.

32. Lamarch, C. P., S. Mousseau, P. Paultre and J. Proulx, "A Comparison of Ambient and Forced-Vibration Testing of a Full Scale Concrete Structure", *Conference: 2004 IMAC-XXII: Conference & Exposition on Structural Dynamics*, 2004.

33. Reynders, E., "System Identification Methods for (Operational) Modal Analysis: Review and Comparison", *Archives of Computational Methods in Engineering*, Vol. 19, No. 1, pp. 51–124, 2012.

34. Khatibi, M. M., M. R. Ashory, A. Malekjafarian and R. Brincker, "Mass–Stiffness Change Method for Scaling of Operational Mode Shapes", *Mechanical Systems and*

Signal Processing, Vol. 26, pp. 34–59, 2012.

35. *Structural Vibration Solutions – Operational Modal Analysis Software Provider*, 1999, `http://www.svibs.com/products/index.aspx`, Accessed at April 2013.

36. *Step Detection*, 2011, `http://en.wikipedia.org/wiki/Step_detection`, Accessed at April 2013.

37. James, G. H., T. T. Cao, V. A. Fogt, R. L. Wilson and T. J. Bartkowicz, "Extraction of Modal Parameters From Spacecraft Flight Data", *Loads and Structural Dynamics Branch NASA Johnson Space Center & The Boeing Company Space Exploration Division*.

38. Rainieri, C., G. Fabbrocino, G. Manfredi and M. Dolce, "Robust Output-Only Modal Identification and Monitoring of Buildings in the Presence of Dynamic Interactions for Rapid Post-Earthquake Emergency Management", *Engineering Structures*, Vol. 34, pp. 436–446, 2012.

39. Hans, S., C. Boutin, E. Ibraim and P. Roussillon, "In-Situ Experiments and Seismic Analysis of Existing Buildings. Part I: Experimental Investigations", *Earthquake Engineering and Structural Dynamics*, Vol. 34, pp. 1513–1529, 2005.

40. Michel, C., P. Guéguen, P. Lestuzzi and P.-Y. Bard, "Comparison Between Seismic Vulnerability Models and Experimental Dynamic Properties of Existing Buildings in France", *Bulletin of Earthquake Engineering*, Vol. 8, No. 6, pp. 1295–1307, 2010.

41. Shing, P. B. and A. B. Mehrabi, "Behaviour and Analysis of Masonry-Infilled Frames", *Progress in Structural Engineering and Materials*, Vol. 4, No. 3, pp. 320–331, 2002.

42. Köse, M. M., "Parameters Affecting the Fundamental Period of RC Buildings with Infill Walls", *Engineering Structures*, Vol. 31, No. 1, pp. 93–102, 2009.

43. *SAP2000 V15 Advanced, Computers and Structures, Inc.*, 1996, http://www.csiberkeley.com/sap2000, Accessed at April 2013.

44. Canbay, E., U. Ersoy, G. Özcebe, H. Sucuoğlu and S. T. Wasti, *Binalar İçin Deprem Mühendisliği Temel İlkeler*, ODTÜ Geliştime Vakfı Yayıncılık, Ankara, Turkey, 2008.

45. Çağlayan, E., *Betonarme Çerçevelerin Yatay Yüklere Göre Analizinde Dolgu Duvar Etkisinin İncelenmesi*, MSc. Thesis, Celal Bayar University, 2006.

46. *Seismic Evaluation and Retrofit of Concrete Buildings*, 1996, Advanced Technology Council, USA, California.

47. Chopra, A. K. and R. K. Goel, "A Modal Pushover Analysis Procedure for Estimating Seismic Demands for Buildings", *Earthquake Engineering and Structural Dynamics*, Vol. 31, No. 3, pp. 561–582, 2002.

48. Shakeri, K., M. A. Shayanfar and T. Kabeyasawa, "A Story Shear-Based Adaptive Pushover Procedure for Estimating Seismic Demands of Buildings", *Engineering Structures*, Vol. 32, No. 1, pp. 174–183, 2010.

49. Shakeri, K., K. Tarbali and M. Mohebbi, "An Adaptive Modal Pushover Procedure for Asymmetric-Plan Buildings", *Engineering Structures*, Vol. 36, pp. 160–172, 2012.

50. PEER, *Pacific Earthquake Engineering Research Center: NGA Database*, 1999, http://peer.berkeley.edu/nga/earthquakes.html, Accessed at May 2013.

51. AFAD, *Türkiye Ulusal Kuvvetli Yer Hareketi Gözlem Ağı*, 2009, http://kyh.deprem.gov.tr, Accessed at May 2013.

52. CESMD, *Center for Engineering Strong Motion Data*, 2008, http://www.strongmotioncenter.org, Accessed at May 2013.

53. NIED, *National Research Institute for Earth Science and Disaster Prevention*, 1996, `http://www.kyoshin.bosai.go.jp`, Accessed at May 2013.

54. COSMOS, *Consortium of Organizations for Strong Motion Observation Systems*, 1999, `http://www.cosmos-eq.org`, Accessed at May 2013.

55. Strang, G., *Lecture 34: Fourier Integral Transform (Part 2) — Video Lectures — Computational Science and Engineering I*, 2008, `http://ocw.mit.edu/courses/mathematics/`, Accessed at March 2013.

56. Welch, P. D., "The Use of Fast Fourier Transform for the Estimation of Power Spectra: A Method Based on Time Averaging Over Short, Modified Periodograms", *IEEE Transactions on Audio and Electroacoustics*, Vol. 15, No. 2, pp. 70–73, 1967.